

## **1. Principal Investigator** R. Rox Anderson, MD

**Title:** Normalizing Traumatic Scars

### **Objective**

To extend the skin remodeling capabilities of fraxel laser technology to minimize the amount and effects of skin scarring resulting from injuries to military personnel.

### **Approach**

Wellman Center has invented a way to stimulate skin to remodel (renew) itself called fractional laser treatment. With this technique, microscopic laser beams are used to create thousands to millions of very small laser surgical zones. Each zone is a column that can extend up to a centimeter deep, but is smaller than a hair in width. Unlike a macroscopic wound, tissue healing happens very fast and without scarring. The new tissue forms on only the microscopic scale. A single fractional laser treatment can make skin renew up to 50 % of its own volume. The FDA has approved fractional laser treatment, which is now widely available and is already being used in some military medical care centers.

However, the optimal treatment parameters and important details of the mechanisms involved are unknown, and are unlikely to become known simply from clinical practice. We have proposed to perform parametric dose-response studies of scar treatment with fractional laser technologies (ablative and non-ablative versions, both FDA approved for human use), in a swine scar model developed at ISR. This work is to include the following:

1. Establish a swine skin scar model by using an anti-skin-contracting device. After skin scar formation, we will use fractional laser to treat the scar with 2 or 3 doses and 2 different sizes of damaged area. The treated scar samples will be harvested at day 3, 14, 30, and 60 post-treatment. Normal skin and scar without treatment will be collected as the controls.
2. Total RNA will be isolated for preparing mRNA. The mRNA will used for gene array analysis by swine gene array from the Affymetrix.
3. Bioinformatics will be employed for accessing the results of the gene array test. The gene related to scar remodeling or skin regeneration will be grouped.

### **Accomplishments**

Work on this project has been interrupted because a key investigator on the project suffered a personnel tragedy. Her involvement has been central to our progress and her several month absence from active involvement has set us behind schedule. She will be returning to work in the very near future and we do anticipate being able to complete the experiments which had been begun under this project. Those experiments however, will not be completed prior to the expiration of this award.

### **Significance**

Recently, fractional laser treatment has been shown to impressively normalize surgical, trauma and burn scars. Wounded soldiers with scars, especially those with painful hypertrophic burn scars, are already being helped by fractional laser treatment, and we are sharing clinical knowledge with military (especially Air Force) physicians. The work in this proposal will be central to optimizing the application of fractional laser treatment for this specific purpose.

## Report Documentation Page

*Form Approved*  
*OMB No. 0704-0188*

Public reporting burden for the collection of information is estimated to average 1 hour per response, including the time for reviewing instructions, searching existing data sources, gathering and maintaining the data needed, and completing and reviewing the collection of information. Send comments regarding this burden estimate or any other aspect of this collection of information, including suggestions for reducing this burden, to Washington Headquarters Services, Directorate for Information Operations and Reports, 1215 Jefferson Davis Highway, Suite 1204, Arlington VA 22202-4302. Respondents should be aware that notwithstanding any other provision of law, no person shall be subject to a penalty for failing to comply with a collection of information if it does not display a currently valid OMB control number.

1. REPORT DATE <b>31 MAR 2011</b>	2. REPORT TYPE <b>Final</b>	3. DATES COVERED <b>01-02-2004 to 31-12-2010</b>	
4. TITLE AND SUBTITLE <b>Research To Develop Biomedical Applications of Free Electron Laser Technology</b>		5a. CONTRACT NUMBER <b>FA9550-04-1-0079</b>	
		5b. GRANT NUMBER	
		5c. PROGRAM ELEMENT NUMBER	
6. AUTHOR(S) <b>Rox Anderson; Michael Hamblin; Tayyaba Hasan; Irene Kochevar; Charles Lin</b>		5d. PROJECT NUMBER	
		5e. TASK NUMBER	
		5f. WORK UNIT NUMBER	
7. PERFORMING ORGANIZATION NAME(S) AND ADDRESS(ES) <b>Wellman Center for Photomedicine/Massachusetts General Hospital ,55 Fruit St,Boston,MA,02114-2621</b>		8. PERFORMING ORGANIZATION REPORT NUMBER <b>; AFRL-OSR-VA-TR-2011-0213</b>	
9. SPONSORING/MONITORING AGENCY NAME(S) AND ADDRESS(ES) <b>AFOSR, 875 North Randolph Street, Suite 325, Arlington, VA, 22203</b>		10. SPONSOR/MONITOR'S ACRONYM(S)	
		11. SPONSOR/MONITOR'S REPORT NUMBER(S) <b>AFRL-OSR-VA-TR-2011-0213</b>	
12. DISTRIBUTION/AVAILABILITY STATEMENT <b>Approved for public release; distribution unlimited</b>			
13. SUPPLEMENTARY NOTES			
14. ABSTRACT <b>The overall goal is to solve substantial military medical problems by creating technologies that are useful to diagnose and care for soldiers, and by elucidating the mechanisms of organ trauma and diseases that particularly affect soldiers. To achieve this broad goal, we have undertaken projects focused on novel treatments of infectious diseases and physical trauma relevant to military personnel, technological improvements for trauma care, and new approaches to triage. Infectious Diseases. Our approach is based on our experience in developing novel photochemical methods of killing organisms using a combination of molecular delivery systems and light-activated dyes (photosensitizers). Trauma Care. Our approach to improving therapeutic interventions for trauma includes developing new tools for the medic/surgeons. Trauma Triage. Small, fieldable, non-invasive optical probes that assess trauma victims are being developed.</b>			
15. SUBJECT TERMS <b>photodynamic therapy, optical coherence tomography, optical diagnostics, photochemical tissue bonding, laser-tissue interaction, photosensitizers, traumatic brain injury, leishmaniasis, fraxel</b>			
16. SECURITY CLASSIFICATION OF:			17. LIMITATION OF ABSTRACT <b>Same as Report (SAR)</b>
a. REPORT <b>unclassified</b>	b. ABSTRACT <b>unclassified</b>	c. THIS PAGE <b>unclassified</b>	
			18. NUMBER OF PAGES <b>46</b>
19a. NAME OF RESPONSIBLE PERSON			



**Publications**

None

**Patents from this award**

None

**2. Project Investigators:** Michael R Hamblin Ph.D., Tianhong Dai, PhD,  
Liyi Huang PhD

**Project Title:** Photodynamic therapy for *Candida albicans* in infected burns

**Objective**

Patients and casualties with burns covering large areas of their total body surface (>20%) are particularly susceptible to infections in the wounds, and these can frequently develop into septicemia and death. Burns destroy the cutaneous barrier, rendering the affected tissue non-perfused, and bacteria find the burn wound a highly nutritional environment due to the biochemical reactions consequent upon the injury (proteolysis and lipolysis releasing amino acids, glycerol and fatty acids). Suppression of the immune system mediated by interleukin-10 production also predisposes to infection. Rapid proliferation and the ability of the bacteria to invade tissue then allow the infection to progress, finally causing bacteremia and systemic sepsis. Due to the inability of systemically administered antibiotics to penetrate the non-perfused tissue of the burn eschar, topical antimicrobials are frequently employed to combat burn wound infections.

Fungi are important opportunistic pathogens of humans, recently ranking as the seventh most common cause of infectious disease-related deaths in the United States. Opportunistic fungal pathogens may cause superficial or invasive infections. The majority of invasive fungal infections are caused by species of *Candida* and *Aspergillus* and *Cryptococcus neoformans*. Despite the increasing importance of opportunistic fungal pathogens, the number of effective antifungal drugs remains limited, with resistance compromising the effectiveness of all but the newest.

Treatment of these resistant organisms with alternative therapeutic strategies such as PDT may be a valuable addition to present methods, and is the objective of these studies.

**Approach**

The bioluminescent *C. albicans* strain used in this study was CEC 749. The luciferase reporter was constructed by fusing a synthetic, codon-optimized version of the *Gaussia princeps* luciferase gene to *C. albicans* PGA59, which encodes a glycosylphosphatidylinositol-linked cell wall protein. Luciferase expressed from this PGA59-gLUC fusion was localized at the *C. albicans* cell surface<sup>5</sup>, allowing the detection of luciferase in intact cells after the addition of the luciferase substrate, coelenterazine, using bioluminescence imaging. *C. albicans* was routinely grown at 30°C on yeast peptone dextrose (YPD) agar and sub-cultured in YPD medium.

It is known that photosensitizers (PS) with a cationic charge are much more efficient at mediating killing of microorganisms than PS with neutral or anionic charges. This applies to Gram-positive bacteria and to fungi but is most pronounced with Gram-negative bacteria. We have developed a panel of highly effective antimicrobial photosensitizers that possess molecular diversity and flexibility. Most of these molecules possess a marked cationic charge and can therefore bind efficiently and strongly to microbial cells, since both bacteria and fungal cells have pronounced anionic or negative charges. Although much is known about structure-function relationships that

pertain to both Gram-positive bacteria and Gram-negative bacteria, much less is known about the optimal structures for PDT of fungal cells. Photosensitizers as diverse as hematoporphyrin derivative and methylene blue have been reported in the literature.

### Accomplishments

#### Selection of a photosensitizer for in vitro PDT of *C. albicans*

We decided to screen a panel of related photosensitizers that differ in lipophilicity as shown by LogP and hydrophilic/lipophilic balance (HLB). This was conveniently provided by the group of phenothiazinium dyes methylene blue (MB), toluidine blue O (TBO) and new methylene blue (NMB).

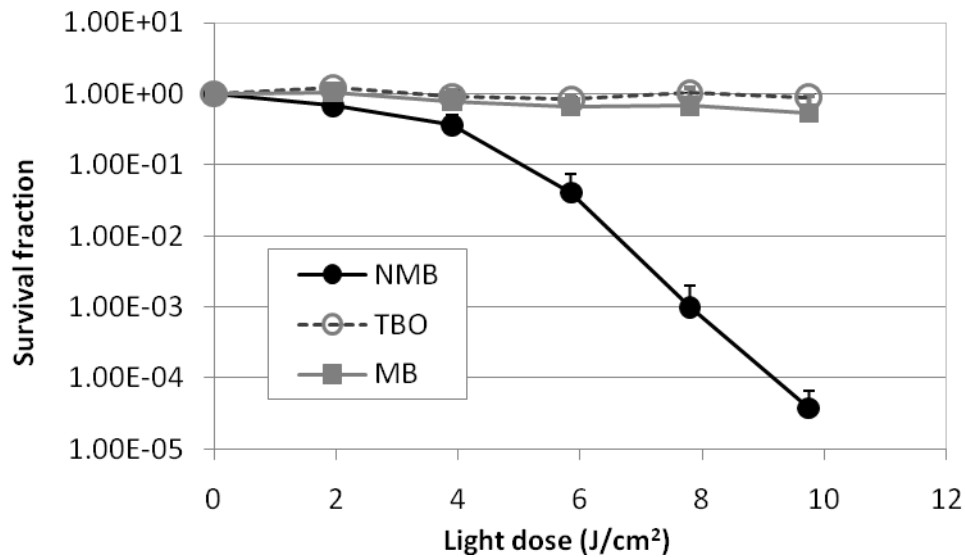


Figure 1. Antifungal photodynamic activity of phenothiazinium dyes with *C. albicans*. Cell suspensions ( $10^7$ /mL) were incubated in the dark at room temperature with  $20 \mu\text{M}$  of the 3 different PS. The suspensions were irradiated with the Lumacare lamp at an irradiance of  $100 \text{ mW/cm}^2$ . During the irradiation, the *C. albicans* suspension was stirred by a mini-magnetic bar. Aliquots of  $50 \mu\text{L}$  of the suspension were withdrawn at 0, 1, 2, 3, 4, and 5 min, respectively. Colony forming units (CFU) were then determined by serial dilution on YPD agar plates by the method of Jett et al. Colonies were allowed to grow for 24-48 hours at  $30^\circ\text{C}$ . Experiments were performed in triplicate for each PS.

It can be seen that NMB was clearly superior (by four orders of magnitude) compared to the other PS, MB and TBO.

#### Development of a mouse model of *C. albicans* infection in third degree burns.

Before the creation of burns, the mice were anesthetized by intraperitoneal (I.P.) injection of a ketamine-xylazine cocktail, shaved on the dorsal surfaces, and then depilated with Nair (Carter-Wallace Inc, New York, NY). Burns were created by applying a single preheated ( $\approx 95^\circ\text{C}$ ) brass block (Small Parts, Inc., Miami, FL) to the dorsal surface of each mouse for 7 seconds, resulting in a nonlethal, full-thickness, third-degree burn. The brass block area was  $10 \text{ mm} \times 10 \text{ mm}$ , giving an area of  $100 \text{ mm}^2$  and corresponding to 2.5% of the total body surface area.

Immediately after the creation of the burns, the mice were resuscitated with I.P. injections of 0.5 mL sterile saline (Phoenix Scientific Inc., St. Joseph, MO) to prevent dehydration.

Fungal infection took place as described by Ha and Jin (25). Five (5) minutes after the creation of the burns (to allow the burns to cool), a suspension (40  $\mu$ L) of *C. albicans* in sterile phosphate buffered saline (PBS) containing 10<sup>6</sup> cells was inoculated onto the eschar of each burn with a pipette tip and was then smeared onto the eschar with an inoculating loop. The mice were imaged with the luminescence camera immediately after the application of the *C. albicans* to ensure that the fungal inoculum applied to each burn was consistent.

An ICCD photon-counting camera (Model C2400-30H; Hamamatsu Photonics, Bridgewater, NJ) was used for bioluminescence imaging. The camera was mounted in a light-tight specimen chamber, fitted with a light-emitting diode, a set-up that allowed for a background gray-scale image of the entire mouse to be captured. By accumulating many images containing binary photon information (an integration time of 2 minutes was used), a pseudo-color luminescence image was generated. Superimposition of this image onto the gray-scale background image yielded information on the location and intensity in terms of photon number. Argus-50 control program (Hamamatsu Photonics) was used to acquire images and to analyze the image data collected.

Prior to imaging, mice were anesthetized by I.P. injections of ketamine/xylazine cocktail. Twenty  $\mu$ L coelenterazine (Gold Biotechnology, Inc, St. Louis, MO; 500  $\mu$ g/mL in 1:9 methanol-PBS) was topically applied to the eschar of each infected burn. Mice were then placed on an adjustable stage in the specimen chamber, and the infected burns were positioned directly under the camera. A gray-scale background image of each wound was made, and this was followed by a photon count of the same region. This entire burn photon count was quantified as relative luminescence units (RLUs) and was displayed in a false color scale ranging from pink (most intense) to blue (least intense).

#### Chronic *C. albicans* infection was developed in mouse burns as characterized by bioluminescence imaging and histological evaluation.

By applying 10<sup>6</sup> CFU of *C. albicans* in PBS topically onto the 7-second burns made on the shaved backs of adult female BALB/c mice, a stable and chronic infection was developed as characterized by bioluminescence imaging. Figure 2A shows the successive bioluminescence images of a representative mouse burn infected with *C. albicans*. After infection, the bioluminescence remained strong and stable until day 12 before the scab peeled off from the mouse back. In all the mice examined in the study, almost no remaining fungal bioluminescence was detected from the burns after the scabs peeled-off, but the detached scabs were all detected as bioluminescent immediately after they came off (Figure 3B). Figures 2C and 2D show representative periodic acid-Schiff (PAS)-stained histological sections of *C. albicans* infected mouse burns biopsied on day 1 and day 4 post-infection, respectively. Massive *C. albicans* invasion was demonstrated on both days by numerous conidia and hyphae branching out in every direction in the burned tissue.

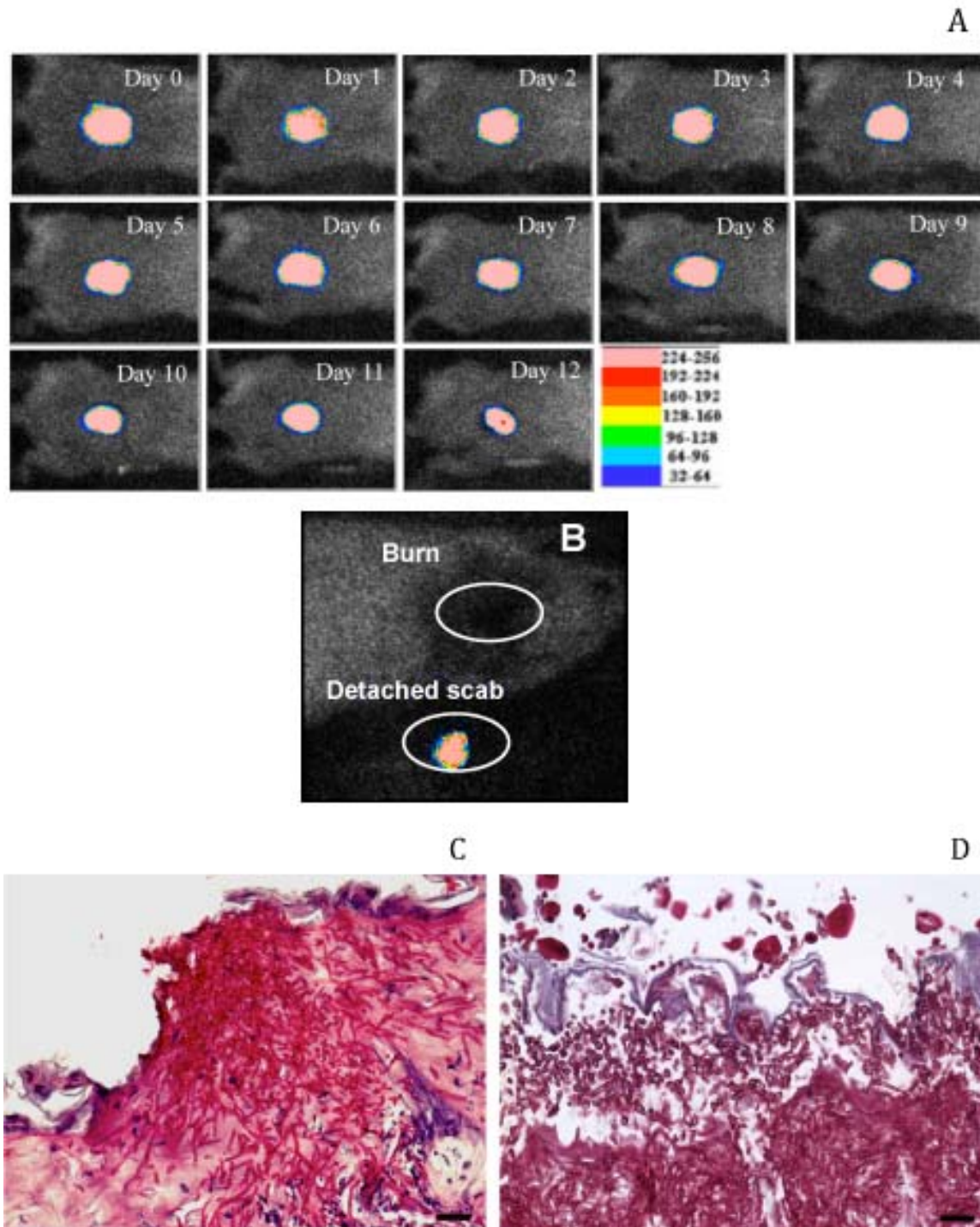


**Figure 3** A) Successive bioluminescence images captured daily for 12 days of a representative mouse burn infected with bioluminescent *C. albicans*. B) A representative bioluminescence image of a mouse burn immediately after the peel-off of its scab as well as the detached scab from the same mouse. C)-D) Representative periodic acid–Schiff (PAS)-stained histological sections of *C. albicans* infected mouse burns biopsied on day 1 and day 4 post-infection, respectively. Scale bars: 20  $\mu$ m.

### PDT of *C. albicans* infected burns

PDT was initiated either at 30 minutes or at 24 hours after fungal inoculation to investigate the therapeutic efficacies of PDT for both early-stage and established infections. NMB solution (100  $\mu$ L of 1mM in PBS) was applied to the surface of the burn and allowed to incubate for 15 min. Light delivery was from Lumacare lamp at wavelength of 660-nm and an irradiance of 100 mW/cm<sup>2</sup>. Mice were given a total light exposure of up to 160 J/cm<sup>2</sup> in aliquots with bioluminescence imaging taking place after each aliquot of light. To record the time course of the extent of fungal infection, fungal luminescence from mouse wounds was captured daily after PDT until the infections were cured (characterized by the disappearance of fungal luminescence) or the burns healed.

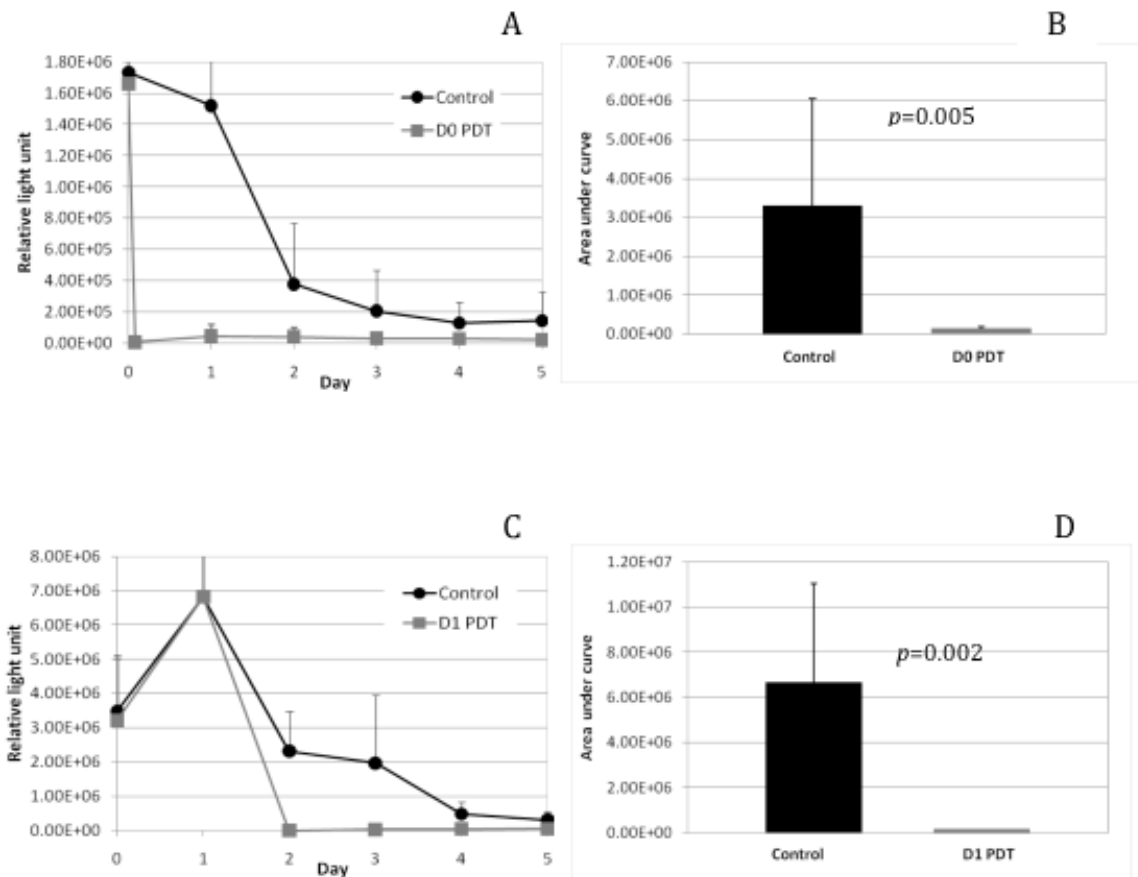


Figure 3. Time courses of mean fungal luminescence of the mouse burns infected with 10(6) CFU of *C. albicans* and treated with PDT on day 0 (30 min after fungal inoculation, n=11) and without treatment (n=11), respectively. B) Mean areas under the bioluminescence-time plots (in the two-dimensional coordinate system in panel A) n=11) and without treatment (n=11), respectively. D) B) Mean areas under the bioluminescence-time plots (in the two-dimensional coordinate system in panel A, day 1 PDT vs. no treatment, p=0.003). Bars are standard deviations.

### **Significance**

PDT for localized infections in burns has a potentially wide area of application. In order to maximize the utility of this therapeutic approach it is necessary to have specific and powerful antimicrobial PS. In burn infections and infections in crushed and lacerated tissue the presence of non-viable tissue and the consequent lack of perfusion due to compromised capillaries reduces

the effectiveness of systemically delivered antibiotics, thus necessitating the application of topical antimicrobial therapy such as PDT. In addition the inexorable worldwide increase in resistance of bacteria and fungi to antibiotics and antifungals has increased the urgency of the search for novel antimicrobial strategies to which bacteria are unlikely to develop resistance. In several experiments PDT has been shown to not cause development of resistance after several cycles of sub-total PDT killing and regrowth. Light based antimicrobial therapies may have the additional beneficial effect of stimulating wound healing.

### **Publications and Abstracts**

1. Dai T, Huang Y-Y, Hamblin MR. Photodynamic therapy for localized infections – state of the art. *Photodiagn Photodyn Ther*. 2009, 6, 170-188. PMC2811240
2. Huang L, Terakawa M, Zhiyentayev T, Huang Y-Y, Sawayama, Y, Jahnke A, Tegos, GP, Wharton T, Hamblin MR. Innovative cationic fullerenes as broad-spectrum light-activated antimicrobials. *Nanomedicine: Nanotechnology, Biology, and Medicine*, 2010, 6(3), 442 – 452. PMC2879475
3. Dai T, Tegos GP, Zhiyentayev T, Mylonakis E, Hamblin MR. Photodynamic Therapy for Methicillin-Resistant *Staphylococcus aureus* Infection in a Mouse Skin Abrasion Model. *Lasers Surg Med*; 2010, 42: 38–44. PMC2820267
4. Coleman JJ, Okoli I, Tegos GP, Holson E, Wagner FF, Hamblin MR, Mylonakis E. Characterization of plant-derived saponin natural products against *Candida albicans*. *ACS Chem Biol*, 2010, 5(3):321-332. NIHMS232376
5. Ragas X, Dai T, Tegos GP, Agut M, Nonell S, Hamblin MR. Photodynamic inactivation of *Acinetobacter baumannii* using phenothiazinium dyes: in-vitro and in-vivo studies. *Lasers Surg Med*; 2010, 42:384–390. NIHMS232374
6. Kishen A, Upadya M, Tegos GP Hamblin MR. Efflux pump inhibitor potentiates photodynamic inactivation of *Enterococcus faecalis* biofilm. *Photochem Photobiol*. 2010. epub ahead of print DOI: 10.1111/j.1751-1097.2010.00792.x
7. Dai T, Huang YY, Sharma SK, Hashmi JT, Kurup DB Hamblin MR. Topical Antimicrobials for Burn Wound Infections. *Recent Patents on Anti-Infective Drug Discovery*, 2010, 5(2):124-51. NIHMS232370
8. Hamblin MR, Dai T. Can surgical site infections be treated by photodynamic therapy? *Photodiagnosis Photodyn Ther*, 2010, 7(2): 134-136. NIHMS232373
9. Huang L, Huang YY, Mroz P, Tegos GP, Zhiyentayev T, Sharma SK, Lu Z, Balasubramanian T, Krayner M, Ruzié C, Yang E, Kee HL, Kirmaier C, Diers JR, Bocian DF, Holten D, Lindsey JS, Hamblin MR. Stable Synthetic Cationic Bacteriochlorins As Selective Antimicrobial Photosensitizers. *Antimicrob Agents Chemother*, 2010, 54; 3834–3841
10. Huang L; Dai T; Hamblin MR. Antimicrobial photodynamic inactivation and photodynamic therapy for infections. *Methods Mol Biol*. 2010, 635: 155-73. PMC2933785
11. Garcez AS, Nunez SC, Hamblin MR, Suzuki H, Ribeiro MS. Photodynamic therapy associated with conventional endodontic treatment in patients with antibiotic resistant microflora. A Preliminary report. *J Endodont*, 2010; 36(9): 1463-1466. doi:10.1016/j.joen.2010.06.001
12. Chiang LY, Padmawar PA, Rogers-Haley JE, So G, Canteenwala T, Thota S, Tan LS, Pritzker K, Huang YY, Sharma SK, Kurup DB, Hamblin, MR. Wilson BC, Urbas A.

- Synthesis and characterization of highly photoresponsive fullereryl dyads with a close chromophore antenna–C60 contact and effective photodynamic potential. *J Mater. Chem.*, 2010, 20, 5280 - 5293, DOI: 10.1039/c0jm00037j
13. Lu Z, Dai T, Huang L, Kurup DB, Tegos GP, Jahnke A, Wharton T, Hamblin, MR. Photodynamic therapy with a cationic functionalized fullerene rescues mice from fatal wound infections. *Nanomedicine UK*. 2010; 5(10):1525-33.
  14. Dai T, Tegos GP, St. Denis TG, Anderson D, Sinofsky E, Hamblin, MR. Ultraviolet-C Irradiation for Prevention of Central Venous Catheter Related Infections: An In-vitro Study. *Photochem Photobiol*. 2010, doi: 10.1111/j.1751-1097.2010.00819.x. [Epub ahead of print]
  15. Ragàs X, Sánchez-García D, Ruiz-González R, Dai T, Agut M, Hamblin MR, Nonell S. Cationic Porphycenes as Potential Photosensitizers for Antimicrobial Photodynamic Therapy. *J Med Chem*. 2010, 53(21):7796-7803.
  16. Garcez SG, Núñez SC, Baptista MS, Daghasanli NA, Itri R, Hamblin MR, Ribeiro MS. Antimicrobial mechanisms behind photodynamic effect in the presence of hydrogen peroxide. *Photochem Photobiol Sci*, 2010 epub ahead of print.
  17. Dai T, Kharkwal GB, Zhao J, St Denis TG, Wu Q, Xia Y, Huang L, Sharma SK, d'Enfert C, Hamblin MR. Ultraviolet-C Light for Treatment of *Candida albicans* Burn Infection in Mice. *Photochem Photobiol*. 2011 Jan 5. epub ahead of print
  18. St Denis TG, Huang L, Dai T, Hamblin MR. Analysis of the Bacterial Heat Shock Response to Photodynamic Therapy-Mediated Oxidative Stress. *Photochem Photobiol*. 2011 Jan 24. doi: 10.1111/j.1751-1097.2011.00902.x epub ahead of print
  19. Huang L, Zhiyentayev T, Xuan Y, Azhibek D, Kharkwal GB, Hamblin MR. Photodynamic inactivation of bacteria using polyethylenimine–chlorin(e6) conjugates: Effect of polymer molecular weight, substitution ratio of chlorin(e6) and pH. *Laser Surg Med*, 2011, in press
  20. Fiamegos YC, Kastiris PL, Exarchou V, Han H, Bonvin MJ, Vervoot J, Lewis K, Hamblin MR, Tegos GP. Antimicrobial and efflux pump inhibitory activity of caffeoylquinic acids from *Artemisia absinthium* against Gram-positive pathogenic bacteria. *PLoS ONE*, 2011, in press
  21. Wainwright M, Dai T, Hamblin MR. Antimicrobial photodynamic therapy in the colon: delivering a light punch to the guts? *Photochem Photobiol*, 2011, in press
  22. Tanaka M, Kinoshita M, Yoshihara Y, Shinomiya N, Seki S, Nemoto N, Hamblin MR, Morimoto Y. Photodynamic therapy using intra-articular Photofrin for murine MRSA arthritis: biphasic light dose response for neutrophil-mediated antibacterial effect. *Laser Surg Med*, 2011, in press.

#### **Patents from this award**

None

**3. Principal Investigator:** Michael R Hamblin Ph.D., QiuHe Wu MD, Ph.D., Tianhong Dai, PhD, Weijun Xuan, MD, PhD, Ying-Ying Huang MD

**Project Title:** Low-level light therapy for traumatic brain injury (TBI)

#### **Objective**

Despite many experimental studies and clinical trials, therapies for acute and/or chronic TBI

remain elusive. Low-level laser (or light) therapy (LLLT) applied transcranially (from outside the skull) has been used successfully in animal models of stroke and in two human phase 3 trials for stroke. This innovative project was designed to test the hypothesis that noninvasive near-infrared transcranial LLLT can be used to treat TBI in the acute and/or chronic settings. Mechanistic studies were performed using cultured cortical neurons, and LLLT was tested in acute and chronic mouse models of TBI.

### Approach

Animal models of TBI can be broadly classified as: 1) impact acceleration models; 2) inertial (nonimpact) acceleration models; or 3) direct brain deformation models. Impact acceleration models involve direct head impacts using a piston, humane stunner or captive bolt pistol, calibrated pendulum, or weight drop onto the skull. Inertial acceleration models involve acceleration of the head without impact. Direct brain deformation models include both fluid percussion and rigid indentation types and use either a fluid pulse or mechanically driven piston, respectively, to rapidly compress the exposed dura or cortex through a craniotomy site. TBI was produced in mice by two different methods. The first is based on the closed head weight drop protocol of Marmarou et al. The second was a controlled cortical impact model using a hydraulically driven piston operating through a craniotomy opening to directly impact the cortical surface.

### Accomplishments

Specific Aim 1 Study mechanisms of LLLT using an in vitro model of cultured primary mouse cortical neurons:

Embryonic mice were sacrificed to allow cells to be isolated from their brains. Depending on whether cytosine arabinoside was used or not (this drug selectively kills proliferating cells) we were able to isolate pure neurons or a mixed neuronal/glial cell culture. Primary cortical neurons were isolated from day 15-16 mouse embryos. Neurons were illuminated with a wide range of fluences (0.03, 0.3, 3, 10 and 30 J/cm<sup>2</sup>) of CW 810-nm laser delivered at 25 mW/cm<sup>2</sup>. Assays were carried out for intracellular levels of reactive oxygen species (MitoSOX red, Figure 1), nitric oxide release (DAF-FM, Figure 2), intracellular calcium (Fluo-4, Figure 3), and mitochondrial membrane potential (MMP, JC1 red/green ratio, Figure 4) Adenosine triphosphate (ATP) was measured by luciferase assay (Cell-Titer-Glo, Figure 5).

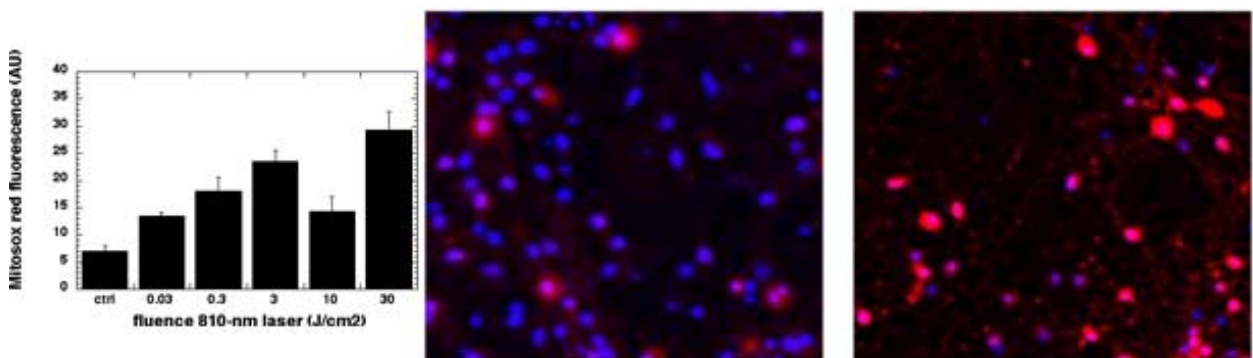


**Figure 1.** Effect of 810-nm laser on production of mitochondrial ROS in the murine cortical neurons. At all fluences, the increase in ROS levels was significantly higher than the control.

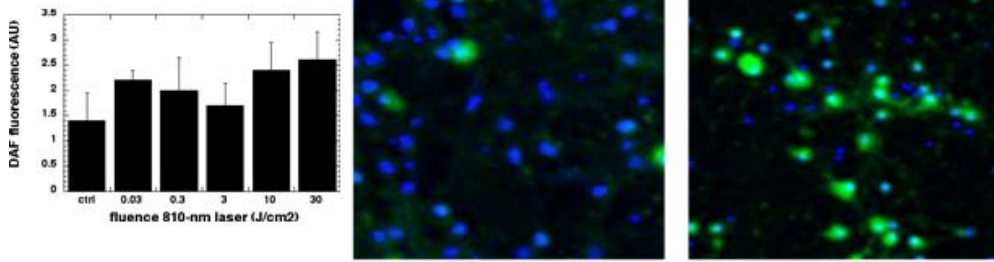


**Figure 2.** Laser induced increase in the NO levels in the primary cortical neurons. A modest increase in NO levels was seen at all the light doses.

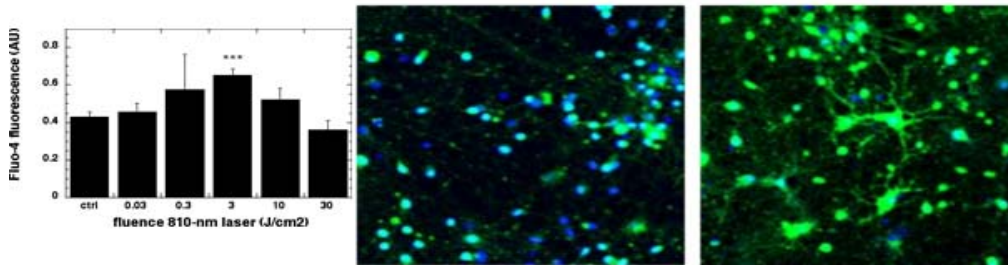


**Figure 3.** Effect of 810 nm laser on the intracellular calcium levels. Lower doses of light induced an increase in  $[Ca^{2+}]_i$  while the levels decline at higher dose.

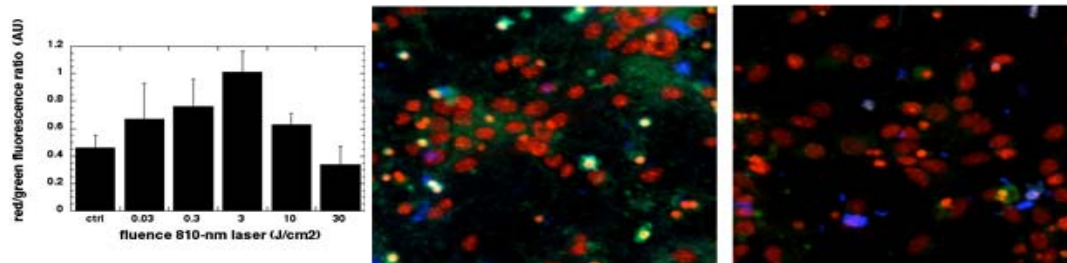


**Figure 4.** Changes in MMP in response to laser irradiation. The MMP increased at fluences  $\leq 10$  J as compared to control but there is depolarization when irradiated with 30 J/cm<sup>2</sup>.

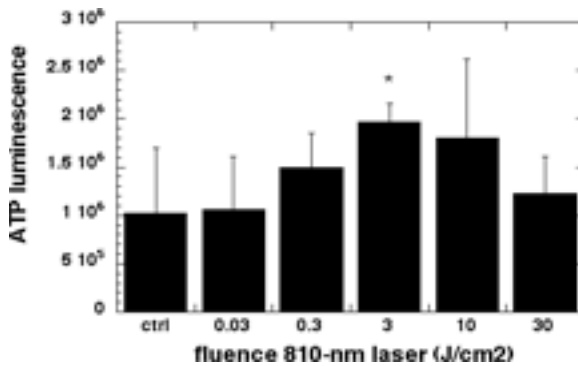


**Figure 5.** ATP levels in the primary neurons irradiated with 810 nm laser. Laser induced ATP synthesis at lower light doses while a decline in ATP was observed at higher dose of light.

Light induced a significant increase in all five markers (ROS, NO, calcium, MMP and ATP) at lower fluences (0.3 to 3 J/cm<sup>2</sup>) and a decrease at higher fluences (10 J/cm<sup>2</sup>). This biphasic dose response is typical of many observations made in vitro when LLLT has been applied to different cultured cells and various assays carried out. ROS and nitric oxide appeared to exhibit 2 peaks; one peak coincided with the peak from group 1 (3 J/cm<sup>2</sup>) while there was a drop in ROS and NO at 10 J/cm<sup>2</sup> but a second peak appeared at 30 J/cm<sup>2</sup>. We interpret this data to mean that at low fluences mitochondrial respiration was stimulated as shown by the increase in ATP, Ca<sup>2+</sup> and MMP and this led to the generation of low amounts of ROS and NO that were able to activate signaling pathways and gene transcription without being enough to cause cytotoxicity. At 10 J/cm<sup>2</sup> the stimulation was reduced because instead of activating mitochondrial respiration, damage to the enzymes began to manifest itself. At 30 J/cm<sup>2</sup> severe damage to the mitochondria began to manifest itself leading to a second large release of ROS and NO and presumably (although it was not measured in this study) apoptosis and cytotoxicity.

The triphasic nature of these ROS and NO responses with increasing fluence may have a bearing on the biphasic dose response of LLLT in general [1].

Specific Aim 2 Test the hypothesis that administration of LLLT in the acute post-injury period will improve cognitive and neurological function after traumatic brain injury in mice.

We tested LLLT in a mouse model of TBI produced by a controlled weight drop onto the closed skull. Mice received a single treatment with one of four different continuous wave lasers: 665-nm, 730-nm, 810-nm or 980-nm (36 J/cm<sup>2</sup> delivered at an irradiance of 150 mW/cm<sup>2</sup> over 4 minutes) given at four hours post-injury and were followed up by neurological performance testing for 4 weeks. Mice with moderate to severe TBI treated with 665-nm and 810-nm laser had a significant improvement in neurological score over the course of the follow-up. The neurological status of the traumatized mice was evaluated at different time intervals after closed head injury according to a neurological severity score (NSS). The neurological tests are based on the ability of the mice to perform 10 different tasks that evaluate the motor ability, balancing, and alertness of the mouse. One point is given for failing to perform each of the tasks; thus, a normal, uninjured mouse scores 0. The severity of injury is defined by the initial NSS, evaluated 1 h post-CHI, and is a reliable predictor of the late outcome.

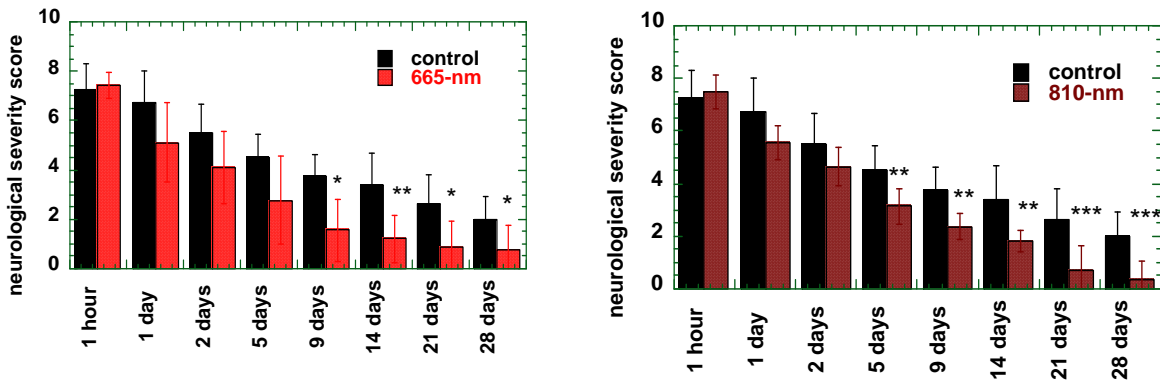


Figure 6. Successive neurological performance testing of mice that received a closed head TBI followed 4 hours later by a single transcranial laser treatment (either 665-nm or 810-nm).

### Specific Aim 3

We tested transcranial LLLT in a different model of TBI called controlled cortical impact (CCI). Here the scalp is opened and a hole is drilled in the skull. The bone piece is removed and a pneumatic piston is released with calibrated force to create a controlled injury to the right cortex of the mouse. The skull is sealed and the scalp is sutured and 4 hours later laser is applied. Figure 8A shows that a single application of 810-nm laser at 50 mW/cm<sup>2</sup> to deliver 36 J/cm<sup>2</sup> at 4 hours post-TBI had significant effects in improving NSS throughout the length of the experiment (4 weeks). Interestingly the beneficial effects of the therapy became more pronounced the longer the mice were followed suggesting that the laser stimulated reparative processes in the brain that took some time to complete. Delivering 14 daily laser treatments however, was of no significant long-term benefit aside from a transient benefit up to 5 days post-TBI. This is an example of the biphasic dose response that is frequently seen in LLLT. Figure B shows another example where we see that a single laser exposure of 36 J/cm<sup>2</sup> at 50 mW/cm<sup>2</sup> is somewhat better than 36 J/cm<sup>2</sup> at 500 mW/cm<sup>2</sup> and much better than 360 J/cm<sup>2</sup> at 500 mW/cm<sup>2</sup>. Finally Figure 8C shows a significant reduction in lesion size at 4 weeks from LLLT treated TBI brains compared to untreated TBI brains.

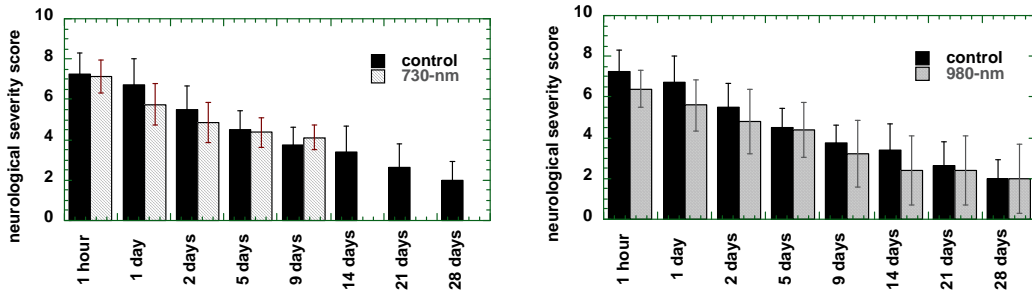


Figure 7. Successive neurological performance testing of mice that received a closed head TBI followed 4 hours later by a single transcranial laser treatment (either 730-nm or 980-nm).

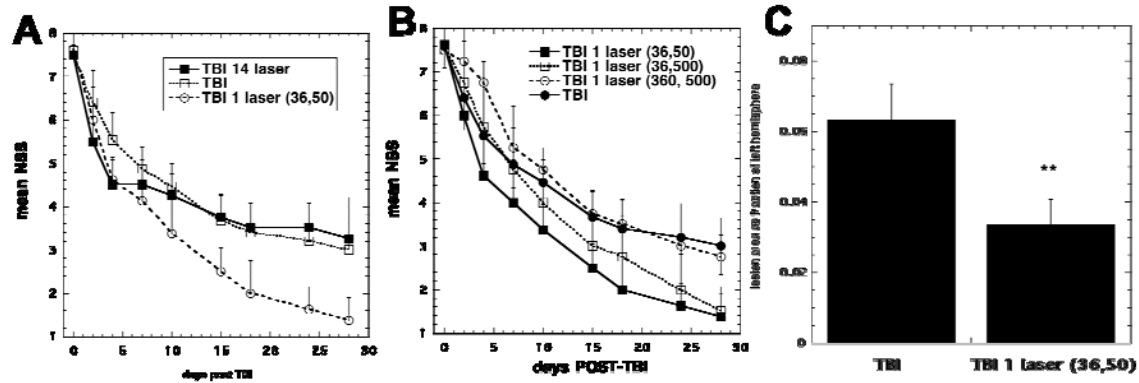


Figure 8. (A) NSS scores from CCI TBI mice untreated or treated with 1 or 14 daily laser exposures. (B) NSS scores from CCI TBI mice untreated or treated with 1 laser exposure delivering 36 J/cm<sup>2</sup> at 50 mW/cm<sup>2</sup>, 36 J/cm<sup>2</sup> at 500 mW/cm<sup>2</sup> or 360 J/cm<sup>2</sup> at 500 mW/cm<sup>2</sup>. (C) Mean lesion area as a fraction of right hemisphere of brains removed from untreated TBI mice or 1 laser Tx at 4 weeks post-TBI.

### Significance

TBI appears to account for a larger proportion of casualties among surviving soldiers wounded in combat in Iraq and Afghanistan, than it has in other recent U.S. wars. As insurgents continue to attack U.S. troops in Iraq, most brain injuries are being caused by improvised explosive devices (IED), and closed brain injuries outnumber penetrating ones among patients seen at Walter Reed, where more than 450 patients with TBI were treated between January 2003 and February 2005. A blast creates a sudden increase in atmospheric pressure by heating and accelerating air molecules and resulting in an initial overpressurization and then immediately thereafter, a sudden decrease in pressure that produces intense wind (an underpressurization). Injuries occur as a direct result of from objects put in motion by the blast that then hit people (secondary blast injury) causing fragmentation injuries and penetrating trauma, and by individuals themselves being put in motion by the blast and then hitting something, such as the ground or inside of a military vehicle potentially causing both open and closed head injuries (tertiary blast injury) Blast injury can cause direct brain concussion, contusions and/or hypoxia (resulting from gas emboli) as a result of the primary blast. Diffuse axonal injuries are common following closed head injuries. These injuries result when shearing, stretching, and/or angular forces pull on axons and small vessels. Impaired axonal transport leads to focal axonal swelling and (after several hours) may result in axonal disconnection. Pathological studies in brain-injured animals (and limited postmortem studies in humans) suggest that TBI typically causes damage to nerve axons in many areas of the brain termed diffuse axonal injury. Excitotoxicity and oxidative stress have been suggested as possible mechanisms of cell injury.

### Publications and Abstracts (4/10-3/11):

1. Wu Q, Huang Y-Y, Dhital S, Sharma SK, Chen A C-H, Whalen MJ, Hamblin MR. Low level laser therapy for traumatic brain injury. In: Hamblin MR, Anders JJ, Waynant RW, Editors. Mechanisms for Low-Light Therapy V, Bellingham, WA, The International Society for Optical Engineering. Proc SPIE 2010, Vol. 7552: 755206-1
2. Huang Y-Y, Chen AC-H, Wu Q, Sharma SK, Hamblin MR. Comparison of cellular responses induced by low level light in different cell types. In: Hamblin MR, Anders JJ, Waynant RW,

- Editors. Mechanisms for Low-Light Therapy V, Bellingham, WA, The International Society for Optical Engineering,. Proc SPIE 2010, Vol. 7552: 75520A-1
3. Chen AC-H, Huang Y-Y, Sharma SK, Hamblin MR. Can dendritic cells see light?. In: Chen WR, Editor; Biophotonics and Immune Responses V, Bellingham, WA, The International Society for Optical Engineering, Proc SPIE 2010, Vol. 7565, 756504-1
  4. Naeser MN, Saltmarche A, Kregel MH, Hamblin MR, Knight JA. Transcranial LED therapy for cognitive dysfunction in chronic, mild traumatic brain injury: Two case reports. In Hamblin, M.R., Anders, J.J. and Waynant, R.W., eds. Mechanisms for Low-Light Therapy V, The International Society for Optical Engineering., Bellingham, WA,. Proc SPIE 2010, Vol. 7552, 75520L-1
  5. Kharkwal GB, Sharma SK, Huang YY, De Taboada L, McCarthy T, Hamblin MR. Effects of 810 nm laser on mouse primary cortical neurons. In: Hamblin MR, Anders JJ, Waynant RW, Editors. Mechanisms for Low-Light Therapy VI, Bellingham, WA, The International Society for Optical Engineering, Proc SPIE 2011. In press.
  6. Chen AC, Huang YY, Sharma SK, Hamblin MR. Effects of 810-nm Laser on Murine Bone-Marrow-Derived Dendritic Cells. Photomed Laser Surg. 2011 Jan 8. epub ahead of print
  7. Naeser MA, Saltmarche A, Kregel MH, Hamblin MR, Knight JA. Improved Cognitive Function After Transcranial, Light-Emitting Diode Treatments in Chronic, Traumatic Brain Injury: Two Case Reports. Photomed Laser Surg. 2010 Dec 23. epub ahead of print
  8. Spagnolli E, Anderson RR, Hamblin MR, Nagasaka Y, Bloch KD, Zapol WM. Protective effects of Red/Near Infrared Radiation on Murine Cardiac Ischemia/Reperfusion Injury. Experimental Biology 2010, Anaheim CA.FASEB J. 2010 24:lb410.
  9. Hamblin MR, Naeser MN, Schiffer F, Wu Q, Huang YY, Transcranial laser therapy for acute and chronic traumatic brain injury. 35th Annual Meeting American Society for Photobiology. 2010, Providence RI.

**Patents from this award**

None

#### 4. Principal Investigator: Tayyaba Hasan, Ph.D.

#### Project Title: PDT for Leishmaniasis

**Objective:** Photodynamic therapy (PDT) is a therapeutic approach based on the photo-oxidation of biological materials induced by non-toxic chemicals called photosensitizers (PSs). The PS preferentially localizes in certain diseased cells and these cells are destroyed when illuminated by a light of the right wavelength and at a sufficient PS dose. PDT has evolved as a promising therapeutic modality for the treatment of cutaneous leishmaniasis (CL). The first clinical study of PDT for cutaneous parasitic infections showed that PDT promotes relatively faster localized healing of the diseased lesion. In particular, phenothiazine compounds have demonstrated efficacy for PDT of CL. In previous years, we demonstrated the success of PDT in treatment of CL in an ear model of infection using PS, 3,7-bis(di-n-butylamino)phenothiazin-5-ium bromide, (PPA904). Since the site of infection plays an important role in determining the pathology (*Baldwin et.al; Infections and Immunity, 2003, 6830-34*), the objective of our present study is; (i) to establish a clinically relevant model for PDT by comparing the base of tail (BT) mouse model with ear model of infection, and (ii) to establish the efficacy of a gel formulation

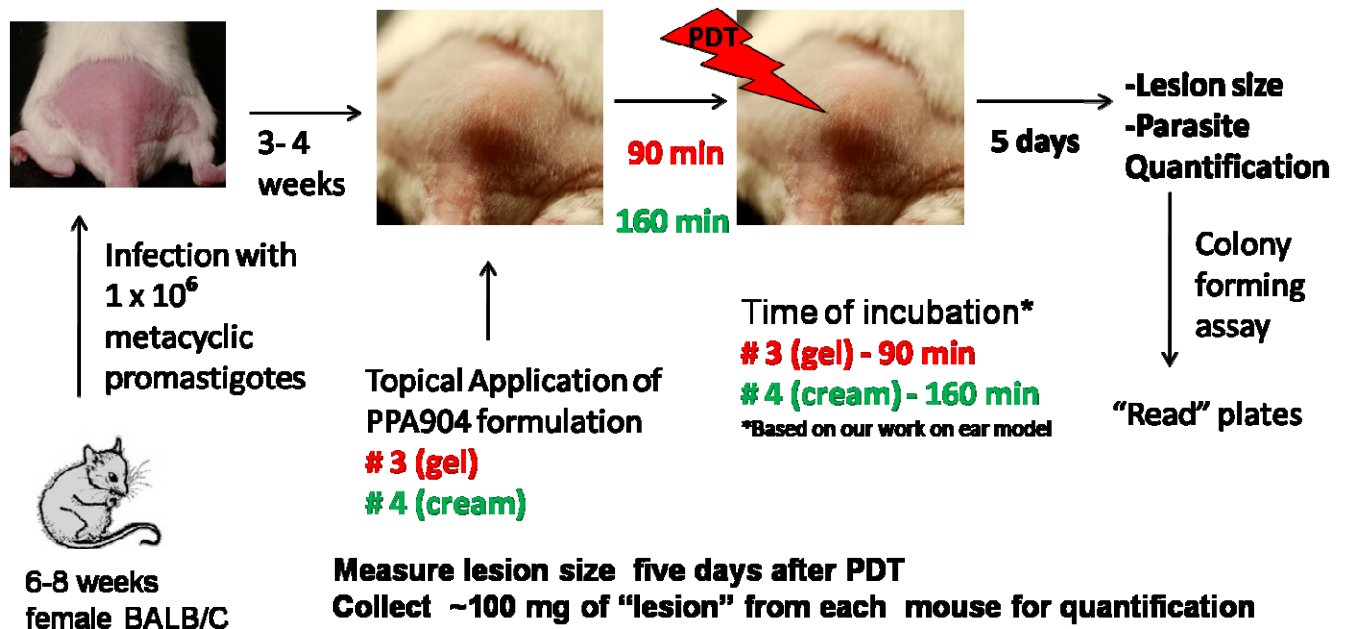


Figure 1: In-vivo PDT of BT infection model

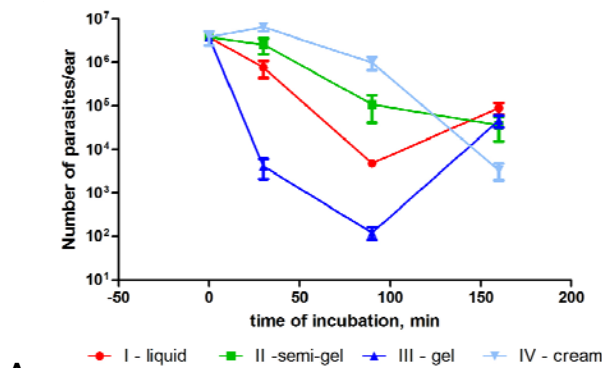
and a cream formulation for PS, PPA904. The BT model yields a thicker lesion providing an infection which may be more similar to a human lesion in some cases.

**Approach:** For in vivo BT study, 6-8 weeks old female BALB/C mice were infected with  $1 \times 10^6$  metacyclic promastigotes of *L. Major (old world)* strain of Leishmania. The infection was allowed to develop for 3-4 weeks. Two different PPA904 formulations (gel and cream), that have shown good penetration at the site of infection and parasite killing

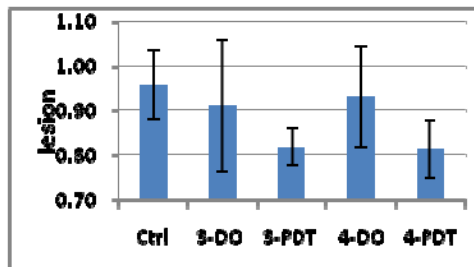
in our previously studied ear model of infection, were used for PDT. As this is our first study with BT model, topical drug application and incubation time points were identical



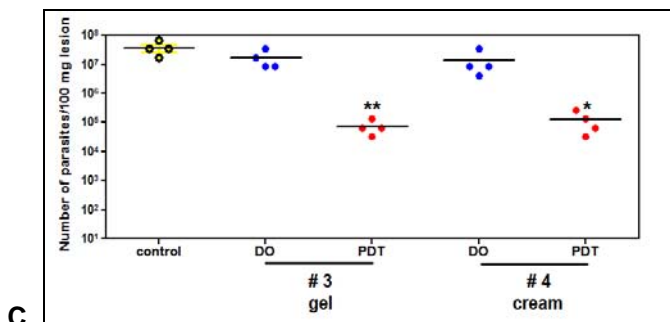
Figure 2: Model Development with *L. Major* strain.



A.



B.



C.

Figure 3: Incubation time (A), lesion size (B) and parasite quantification (C) in *L. major* infection. Incubation time is studied in an ear model of infection, while lesion size and parasite quantification studies are performed on a BT model of infection. Where: Ctrl=control; 3-DO= cream-drug only; 3-PDT= cream-PDT treatment; 4-DO= gel-drug only; and 4-PDT= gel-PDT treatment. N=4

to that used in the ear model of infection. A schematic of infection development, drug application, incubation, and study endpoints are shown in **Figure 1**.

**Accomplishments: A robust and reproducible BT model was developed and a dose dependent parasite reduction was observed.**

The Walter Reed Army Institute of Research helped establish a robust and reproducible BT model in our laboratory.

**Figure 2** shows the *L. Major* infection site at day 9 and 15 following parasite injection.

The treatment was given 3-4 weeks post injection. Our previous work with ear model of infection (**Figure 3A**) indicated that the cream formulation is more effective with increase in incubation time. However, increasing incubation time above 90 minutes does not improve the parasite eradication in gel formulations. Based on this, the gel formulation was applied topically for 90 minutes, and the cream was applied for 160 minutes.

After appropriate incubation, the designated treatment area was irradiated with a broad band light source of  $665 \pm 15\text{nm}$  at a fluence of  $50\text{ J/cm}^2$  ( $50\text{mW/cm}^2$ ). Lesion size was measured 5 days after treatment (**Figure 3B**) and an approximate 15-20 %

reduction in size was observed with a single treatment. The number of parasites in the CL lesions decreased by 2 orders of magnitude for both cream and gel formulation (**Figure 3C**). The results observed with a single PDT regimen in BT model is in range of parasite reduction observed for ear model of infection with both cream and gel formulations. In the previous year, we have shown that more than one PDT treatment significantly improves clinical outcome. To better understand the formulations and their impact at the site of infection, we further plan to establish a multiple treatment protocol in BT model of infection and broaden this study to new world strains, such as *L. panamamensis*.

**Significance:** If successful we anticipate that this research will culminate in a new paradigm for a convenient and safe treatment of leishmaniasis. PDT is efficient and well-tolerated by the patients. PDT is a desirable parasite killing modality because parasites and microbes resistant to standard treatments are responsive to PDT. The best curative PPA904-PDT regimen was achieved under the conditions of a longer duration of topical application time (90 or 160 minutes). While the dynamics of treatment may be somewhat different in humans, we hope that our study with comparison on site of infection and type of formulation will provide a useful starting point for the optimization of topical PDT applications for granulomatous infections.

#### **Publications**

None

#### **Patents from this award**

None

**5. Principal Investigators:** Irene E. Kochevar and Robert W. Redmond

**Project Title:** Attaching biomaterials and tissue constructs

#### **Objective**

The overall goal of this project is to develop light-activated technology to facilitate use of biomaterials and tissue constructs in medicine. A general need in tissue engineering is the ability to secure the biomaterial or construct in a specific tissue location; sutures are often inadequate because of fragility or other property of the material.

#### **Approach**

Our approach is to use photocrosslinking technology that we have developed for other clinical applications. Photocrosslinking involves staining the surfaces to be adhered with a green-absorbing dye then contacting the surfaces. Irradiation with low laser power that does not heat the tissue produces an immediate, strong and water-tight bond. In this project we focused on two aspects, namely, a specific application of bonding a biomaterial (silk) to tissue (tendon) in order to enhance repair and basic studies to understand the underlying molecular mechanisms for photocrosslinking in order to optimize use of this process for tissue engineering.

#### **Accomplishments:**

Specific aim 1: To improve healing rates and restoration of function after tendon repair using photocrosslinking to secure a fiber-aligned electrospun silk mat over the gap.

We have developed electrospun silk nanofiber mats for use in augmentation of surgical tendon repair of Achilles tendon rupture. Silk fibroin is extracted from silkworm cocoons and electrospun to form nanofiber mats of approximately 50  $\mu\text{m}$  thickness and 1  $\mu\text{m}$  fiber diameter. Mechanical testing of these materials yielded breaking strength of  $\sim 4$  MPa and a Young's modulus of 125 MPa. This stiff material is intended to provide added strength to the repair in the initial stages of wound healing when the risk of re-rupture is high. In a clinical setting such added strength to the repair would allow for earlier mobilization of the joint, which has been shown to provide better recovery of function with less stiffness. The ability to provide added tensile strength was evaluated at 7, 14 and 28 days post repair in a rabbit model following complete mid-tendon transection of the Achilles tendon. The 1 x 2 cm silk mats were stained with Rose Bengal, wrapped around the repair site and sealed to the tendon by photochemical crosslinking using 532 nm green light. This group was compared to standard of care surgical repair using sutures only. All repaired limbs were immobilized with a fiberglass cast to prevent mechanical rupture of the repaired tendon. At the study time points, muscle-tendon-bone complexes were harvested and frozen in order to carry out breaking strength measurements at the conclusion of all procedures. Scarring and extent of adhesions were also evaluated. Results showed that both the ultimate stress and Young's modulus of the PTB/silk group was significantly lower than the suture group at early times but recovered to equivalent levels at 28 days post-repair. Significantly, the extent of adhesions from the tendon to surrounding tissue was quantitatively much lower in the PTB/silk group, a clinically relevant observation that suggests a barrier function and potential for less stiffness and improved range of motion. Experiments are now ongoing to evaluate a third group where standard suture repair is augmented with PTB/silk to combine early repair strength with anti-adhesion properties to optimize outcomes.

Specific aim 2. To identify the chemical (functional) groups required for photocrosslinking between polymers (synthetic and natural) and collagen-rich tissues.

Photocrosslinking of collagen initiated by Rose Bengal (RB) photosensitization was investigated using Type I collagen gels as a model for tissues and amniotic membrane, which has a high collagen content. The association of RB with collagen and amnion prior to light activation was assessed by absorption spectroscopy. The results indicated that each collagen triple helix bound up to 15 RB molecules and that, in amnion,  $\sim 80\%$  of the RB associated with loose binding sites and  $\sim 20\%$  associated with tight binding sites. The extent of collagen photocrosslinking after excitation of RB at 532 nm was monitored using SDS-PAGE under conditions in which  $\sim 4$  RB molecules were associated with the collagen triple helix. Collagen dimers, trimers and polymer were produced by photocrosslinking in a fluence-dependent manner. The formation of crosslinked collagen was at least partially dependent on the presence of oxygen. Consistent with this finding, photobonding of amnion to collagen-rich cornea stroma was inhibited by  $>80\%$  when oxygen was removed. A photocrosslinking mechanism that requires the involvement of singlet oxygen was demonstrated. Chemically blocking about 50% of the arginine amino acid side chains in collagen almost entirely reduced crosslink formation. To determine whether the amino acids in the non-helical N- and C-terminal regions of the collagen molecule were involved in photocrosslinks, atelopeptide-collagen (formed by enzymatic degradation of N- and C-terminal regions) was studied. Atelopeptide-collagen quenched the RB fluorescence less than intact collagen but had little affect on the extent of photocrosslinking. These results indicate that the mechanism for light-activated photocrosslinking using RB photosensitization is at least partially oxygen dependent, involves singlet oxygen, requires the presence of arginine side chains and did not require the presence of amino acids in the non-helical regions of collagen. These results are being prepared for publication.

### **Significance**

Photochemical crosslinking of the strong electrospun silk nanofiber mats over the tendon repair site offers the potential of significant strengthening of the initial tendon repair with a reduced suture burden that is likely to reduce complications such as scarring, inflammation and infection. Successful demonstration of these factors at the conclusion of the rabbit study will facilitate translation to clinical studies where early mobilization could be performed with less risk of re-rupture. A better understanding of the light-activated crosslinking mechanism initiated by RB in collagen gels also facilitates the manufacture of optimal collagen-based constructs for use in orthopedic applications, as well as other potential areas like vocal fold repair and corneal crosslinking.

### **Publications and Abstracts**

Two manuscripts are currently being finalized.

1. N. Datta, JL Lowery, WY Oh, T Ni, GC Rutledge, IE Kochevar and RW Redmond. A photoactivated nanofiber material for surgical applications: In vivo study in rat Achilles tendon model.
2. T Ni, K Dubbin, SD Aznar-Cervantes, P Senthil-Kumar, N Datta, MA Randolph, GC Rutledge, IE Kochevar and RW Redmond. A photoactivated nanofiber graft material for augmented Achilles tendon repair.

### **Patents from this award**

None

**6. Principal Investigators:** Irene E. Kochevar and Robert W. Redmond

**Project Title:** Higher Efficiency Light-activated Tissue Repair

### **Objective**

To rapidly close and seal traumatic injuries and surgical wounds with a process that leads to minimal scarring.

### **Approach**

In light-activated tissue repair, a dye (Rose Bengal, RB) is applied to the tissue surfaces, the surfaces are placed in contact and the dye-stained area is exposed to cw 532 nm laser radiation (typically 0.3-0.5 W/cm<sup>2</sup> and 100 - 200 J/cm<sup>2</sup>). An immediate, water-tight bond is produced. The fundamental process underlying our light-activated tissue repair technology is the formation of protein-protein covalent crosslinks that connect the tissue surfaces. In a pilot clinical study, minimal scarring accompanied sealing of excisional wounds and in preclinical studies, little or no fibrosis was observed. These studies focused on the mechanisms underlying the absence or inhibition of scarring and fibrosis that accompanies light-activated tissue repair. Rose Bengal is well known to sensitize cells to light-induced toxicity and thus, if phototoxicity did occur, inflammation and subsequent fibrosis and scarring are likely to result. These studies were designed to investigate why RB is not phototoxic under the treatment conditions used for photobonding since this may underlie the absence of scarring.

### **Accomplishments**

The effects of RB on fibroblasts grown in collagen gels were compared to those on fibroblasts grown as monolayers on tissue culture plates. The collagen gel system was used as a model for dermal cells in tissue. Under conditions in which the fibroblasts contained the same amount of

intracellular RB, the LD<sub>50</sub> for cells grown in collagen gels was ~200-fold higher than that for cells grown as a monolayer indicating that a tissue-like environment protected the cells. Further cell biological studies demonstrated that a major factor in the cells grown in tissue-like conditions was the expression and activation of a cell-survival protein, called Akt. In addition, fibroblasts grown in collagen gels expressed higher levels of certain antioxidant proteins that protect the cells against RB phototoxicity.

We also evaluated the possibility that oxygen depletion, i.e., when processes initiated by the irradiation remove oxygen faster than it diffuses into the substrate, might be occurring in tissue. Since RB phototoxicity is an oxygen-dependent process, depletion of oxygen during the irradiation would protect the cells against phototoxicity. To test for oxygen depletion, the phototoxicity (LD<sub>50</sub>) was measured using a wide range of irradiances. The extent of phototoxicity increased as the irradiance decreased for cells irradiated both in collagen gels or monolayers. Thus, oxygen depletion occurs under the treatment conditions, but does not account for the difference in LD<sub>50</sub> values between cells grown in monolayers and collagen gels. However, this result does indicate that oxygen depletion is likely to be occurring in tissue being treated with light-activated repair. Thus, RB would not be phototoxic when wounds are sealed with PTB and the lack of phototoxicity could contribute to the lack of scarring. The results of these studies are being prepared for publication.

### **Significance**

These results contribute to our understanding of the fundamental processes occurring in tissue during light-activated repair, especially the molecular and cellular mechanisms that inhibit adverse toxic responses that can lead to fibrosis. They aid in development of the technology by providing information to be used to minimize toxicity as we manipulate treatment conditions to enhance bonding efficiency.

### **Publications and Abstracts**

Influence of tissue-mimetic environment on skin cell responses to singlet oxygen. Min Yao, Robert W. Redmond and Irene E. Kochevar, invited presentation at the European Society for Photobiology Annual Meeting, Wroclaw, Poland, September 5-10, 2009 (Abstract)

Influence of tissue-mimetic environment on singlet oxygen-initiated toxicity M. Yao, A. Yaroslavsky, F.P. Henry, R.W. Redmond, I.E. Kochevar, invited presentation at the Mutagenesis and Experimental Pathology Society/Society of Free Radicals Meeting, Sydney Australia Dec 4-7, 2009 (Abstract)

### **Patents from this award**

None

**7. Principal Investigators:** Irene E. Kochevar and Robert W. Redmond

**Project:** PTB Clinical Study

### **Objective**

Test the hypothesis that peripheral nerve injuries repaired with photochemical tissue bonding (PTB) and an amnion nerve wrap heal with less scarring and ultimately improved functional outcome than those treated with the conventional microsurgical repair method.

## **Approach**

A clinical study is planned in collaboration with a plastic surgeon, Dr. Jonathan Winograd, to compare outcomes after repair of digital nerves with PTB/amnion wrap versus microsurgical repair. Up to 38 patients with one or more digital nerve injuries requiring repair will be recruited at MGH. Patients will be randomized to PTB and microsurgical groups. Subjects in the PTB group will undergo repair using only 2 microsutures (compared to 6-8 for microsurgery) followed by wrapping with Rose Bengal-stained amniotic membrane and sealing using 532 nm light at an irradiance of 0.25 W/cm<sup>2</sup>. Study visits will be the treatment day, then post-op six weeks, 3, 6, 9 and 12 months. Non-invasive assessments of nerve regeneration will be undertaken. At 6-week and 12-month visits objective assessment of nerve regeneration by non-invasive sensory nerve conduction studies will be conducted by a neurologist. The ratings of the two clinical tests, the subjects' responses and the neurological evaluations will be analyzed. Appropriate statistical tests will be used for the different endpoints and significance will be set at < 0.05.

## **Accomplishments**

A clinical study protocol was written and collaborations with the occupational therapy department and neurology departments were established for assessing the progress of nerve regeneration. An agreement was made with the plastic surgery service that established the procedure and personnel for identifying and treating patients under this clinical study protocol. The protocol was submitted to the MGH IRB and reviewed. A concern was expressed that the PTB nerve repair treatment might not be an insignificant risk, despite the fact that the dye (Rose Bengal), the clinical laser and amniotic membrane are all FDA cleared. We were advised to clarify the non-significant risk status with the FDA. The licensee of this PTB technology is currently preparing an application to the FDA for use of PTB for a different clinical application. We have been advised to wait for that application to clear before approaching the FDA for the nerve repair study. Consequently, this support was used to expedite the statistical analysis of the results of an ongoing clinical study of PTB for closure of skin excisions.

The results of the PTB/skin excision pilot clinical trial have now been fully analyzed. The objective of that study was to determine the effectiveness of PTB for superficial closure of skin excisions and to compare the results to standard epidermal suturing. A split-lesion, paired comparison study of 31 skin excisions was performed. Following deep closure with absorbable sutures, one-half of each wound was superficially closed with non-absorbable sutures while the other half was stained with Rose Bengal dye and treated with green light. After 2 weeks, PTB-treated segments showed no dehiscence and less erythema than sutured segments as assessed from photos ( $p=0.001$ ) and by onsite physicians ( $p=0.005$ ). Overall appearance after PTB was judged better than after sutures from photos ( $p=0.002$ ). The scar produced by PTB at 6 months was rated better than the scar after sutured closure in appearance ( $p<0.001$ ), width ( $p=0.002$ ) and healing ( $p=0.003$ ) from photos and was rated better by onsite physicians ( $p=0.004$ ). Patients were more satisfied with the appearance of the PTB-sealed wound half after 2 weeks and 6 months ( $p=0.013$ ;  $p=0.003$ ).

## **Significance**

The study of closure of skin excisions demonstrated that a novel light-activated technology produces less visible scars than standard suture closure. This skin closure technique was demonstrated to not damage the tissue. Thus, the studies and analyses carried out during this project period, in addition to being meaningful in their own right, have provided the necessary information to proceed with application to the IRB for the evaluation of the light-activated sealing of peripheral nerve repair sites with the hope that patients will show increased regeneration of nerves and better functional outcomes.

### **Publications and Abstracts**

Henry FP, Cote D, Randolph MA, Rust EAZ, Redmond RW, Kochevar IE, Lin CP, Winograd JM. Real time in vivo assessment of the nerve microenvironment with coherent anti-Stokes Raman scattering microscopy. *Plast Reconstr Surg.* 2009;123(2 Suppl):123S-30S.

Henry FP, Goyal NA, David WS, Wes D, Bujold KE, Randolph MA, Winograd JM, Kochevar IE, Redmond RW. Improving Electrophysiological and Histological Outcomes by Photochemically Sealing Amnion to the Peripheral Nerve Repair Site. *Surgery.* 2009;145(3):313-21. Epub 2009 Jan 25.

Tsao S, Yao M, Henry FP, Tsao H, R.W. Redmond, I.E. Kochevar Light-activated closure of excisional wounds for reduced scarring: a randomized, single-blind, split-lesion study. Abstract. Annual Meeting of the Society for Investigative Dermatology, Atlanta Ga, May 5-8, 2010

Tsao S, Yao M, Henry FP, Redmond RW, Kochevar IE. Clinical study of Photochemical Tissue Bonding for Skin Excisions. Abstract. 2009 European Society for Photobiology Meeting, Wroclaw Poland, September 5-10.

Tsao S, Yao M, Henry FP, Redmond RW, Kochevar IE. Photochemical tissue bonding for closure of excision wounds: a first-in-human clinical trial. Abstract. 2009 Society for Investigative Dermatology Annual Meeting, Montreal, May 3-8.

Tsao S, Yao M, Henry FP, Tsao H, Redmond RW, Kochevar IE. Laser-Activated Excisional Wound Repair with Photochemical Tissue Bonding. Abstract. 2009 American Society for Lasers in Surgery and Medicine Annual Meeting, Washington DC, April 15-21.

Kochevar IE, Redmond RW. An advanced light-activated technology for tissue sealing and repair. 2008. Abstract. Radiation Research Society Annual Meeting, Boston, September 20-25.

### **Patents from this award**

None

## **8. Principal Investigator:** Charles P. Lin, PhD

**Project Title:** Radiation damage to the eye: cellular response and potential treatment

### **Objective**

Ionizing radiation is commonly used for tumor treatments and to prepare patients for bone marrow transplantation. Aside from medical uses, ionizing radiation can pose a threat to human health in the event of a nuclear attack or accident. Ionizing radiation is known to primarily ablate hematopoietic cells, including stem cells, in the bone marrow. However, depending on the received dose, injury after whole body exposure may not be selective to blood forming tissue, but can affect the gut and central nervous system (CNS). Inflammation and breakdown of protective barriers, such as the blood brain barrier of the central nervous system (CNS), may be caused by radiation induced vascular injury.

In the eye, cataract of the lens is the most commonly observed ocular manifestation of radiation injury. Little is known about the effects of radiation exposure on the integrity of the blood retinal barrier (BRB) and, subsequently, on the retinal environment. Radiation-induced damage of the BRB may lead both to recruitment of leukocytes and to the activation of retinal microglia. Microglia are the resident macrophages of the retina that are differentiated from circulating bone marrow derived cells (BMDCs). Two recent studies have investigated engraftment of BMDCs in mice retinæ following radiation damage, with significantly different results. One group observed substantial engraftment rates (1), but a second group protected the heads with lead shields and observed little engraftment (2). While this difference suggests that direct radiation damage of the

retina is required for BMDC engraftment, neither group investigated the effect of radiation on the resident microglia population. Our aim was to elucidate the effects of ionizing radiation on the integrity of the BRB, the resident microglia, and the BMDC engraftment.

### Approach

We have developed a scanning laser ophthalmoscope (SLO) specifically for high-resolution mouse retinal imaging. Here, we used the instrument to visualize retinal microstructure and to track native and transplanted cells simultaneously in order to investigate the effects of gamma radiation. Irradiations were done using a Cesium source Gammacell 40 Exactor Low Dose-Rate Research Irradiator (MDS Nordion, Ottawa, ON, Canada). Total body irradiation (TBI) was performed at sublethal (6.5 Gy) and lethal levels (9Gy), applied in a single dose. In some sublethally irradiated mice, the heads were protected with a 36 mm thick lead shield, attenuating the gamma radiation dose received by the head to 1% of the applied dose.

To investigate the integrity of the BRB, two groups of C57BL/6 mice were irradiated with sublethal dose (TBI) with and without protective headshield, respectively. Fluorescein angiography (FLA), a standard procedure in ophthalmology that assesses damage of blood retinal barrier (BRB) by means of fluorescein leakage, was performed before and daily for three days after the irradiation. Leakage of fluorescein was detected by time-lapse imaging over three minutes and evaluated by measuring image contrast. Contrast was defined as the ratio of the difference between maximum and minimum pixel values over their sum (the Michelson contrast).

To investigate changes in microglia populations, twelve CX3CR1GFP/+ mice were divided into three experimental groups: A) Sublethal, shielded; B) Sublethal, unshielded; and C) Lethal, unshielded. Lethally irradiated mice received bone marrow transplants by intravenous injection of  $4 \times 10^6$  actin-dsRed+ donor bone marrow cells 5 hrs post irradiation. No signs of radiation sickness were observed during the course of the experiments. Retinal imaging was performed before irradiation to establish baseline images and up to 120 days post irradiation. The numbers of native GFP+ microglia and DsRed+ transplanted cells were counted at baseline and at each follow-up time point.

### Accomplishments

#### Evaluation of BRB Integrity

FLA was performed by fluorescein injection on stage while capturing time-lapse images (**Figure 1**). Image contrast in FLA, as a measure of integrity of the BRB, remained well above 70% in sublethally irradiated shielded mice, but markedly decreased in unshielded mice. In unshielded mice, the contrast decreased to as low as 9% of the baseline value (32% on average, **figure 2**).

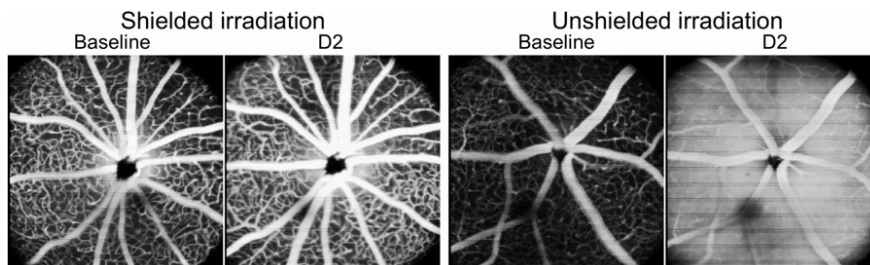
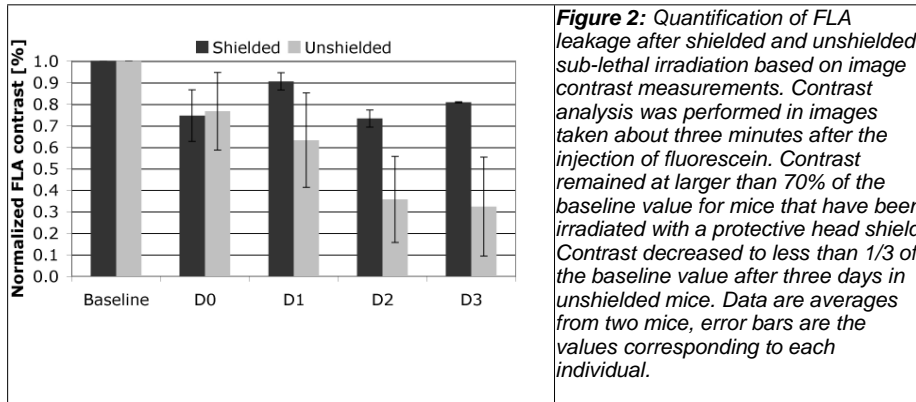


**Figure 1:** Fluorescein angiography (FLA) images after shielded and unshielded sub-lethal irradiation. All images were taken about three minutes after injection of the dye. Contrast in shielded mice was well preserved between baseline and two days after irradiation. Contrast decreased significantly after unshielded irradiation, as compared to baseline.



### Evaluation of Microglial Population

**Figure 3** displays images from three representative mice, one from each experimental condition, followed over the 120-day experimental period. Each image shows a field of view of 30° (approximately 750  $\mu\text{m}$ ) centered on the optic nerve head. Qualitatively, minimal change in the density of GFP<sup>+</sup> microglia density can be perceived in the unshielded sublethally irradiated mice. No change is obvious in the shielded sublethally irradiated mice. However, **Figure 3** demonstrates progressive loss of native, GFP<sup>+</sup> microglia and extravasation of transplanted DsRed<sup>+</sup> cells after lethal irradiation.

Quantitative analysis confirmed a dose dependent loss of resident microglia (**Figure 4a**). Virtually no change in the number of endogenous microglia was detected in mice that received sublethal irradiation with a protective headshield. In contrast, a transient loss in endogenous microglia was detected in mice that were exposed to sublethal irradiation without protection so that at days 28 and 42 microglia numbers were approximately 80% of baseline values. These had returned to normal by day 90. Mice exposed to lethal irradiation without retinal protection suffered progressive loss in retinal microglial cell numbers. By day 28, endogenous microglial cell numbers in this condition were reduced to 61% of baseline values, and by day 120 they were further reduced to 25% of baseline values. However, by day 70 loss of endogenous microglia was compensated partially by migration and engraftment of BM-derived dsRed cells (**Figure 4b**). The number of engrafted dsRed cells doubled between days 70 and 120.

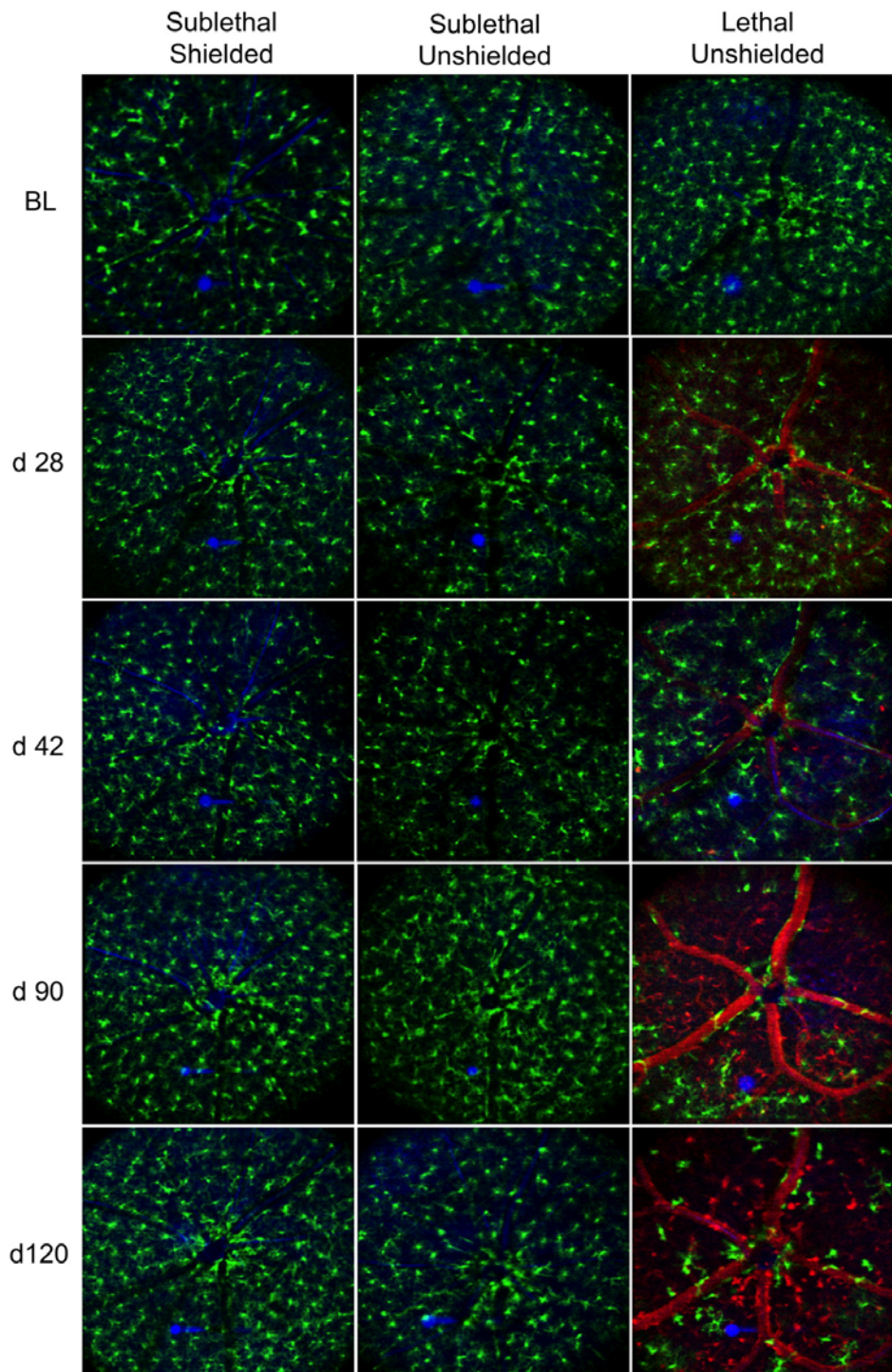


**Figure 3.** Time-course retinal images taken with the SLO from three individual mice subjected to gamma irradiation under different conditions. **Left column:** No loss in microglial numbers is apparent in the retina that was protected from sublethal irradiation. **Middle column:** After sublethal, unshielded irradiation, transient loss in the number of microglia on day 42 can be perceived by reduced microglia density. By day 90 the number of microglia had recovered. **Right column:** In lethally irradiated animals, progressive loss of native microglia and replacement by the BMDC are clearly visible. In these chimeric mice, the vasculature appears fluorescent from circulating dsRed<sup>+</sup> hematopoietic cells. Blue denotes reflectance. Green denotes GFP<sup>+</sup> native

microglia. Red denotes DsRed<sup>+</sup> BMDC. Field of view = 30° (about 750 μm).

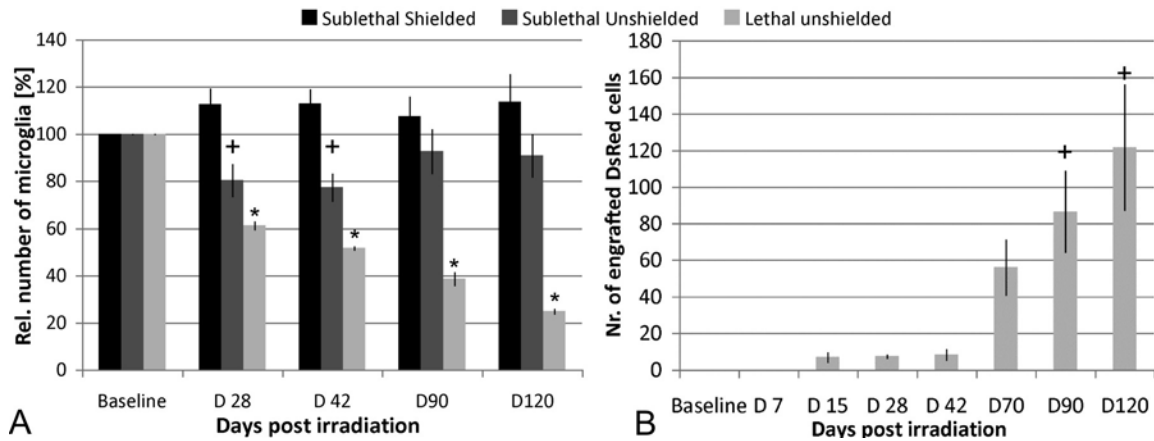


**Figure 4.** Dynamic changes of the microglial population in the retina after gamma irradiation. **(A)** The native GFP<sup>+</sup> microglial population progressively disappeared in lethally irradiated mice. Transient microglial loss was detected in sublethally, shielded mice, but no significant change in numbers was observed in mice that had been sublethally irradiated with head protection. + $P \leq 0.05$ ; \* $P \leq 0.015$  using a paired ttest comparing the numbers of native microglia on individual days post irradiation to the baseline numbers. **(B)** Appearance of BM derived DsRed microglia in the retina after lethal irradiation and BM transplant. Beginning around 70 days post irradiation, significant numbers of DsRed microglia cells extravasated into the retinal parenchyma. + $P \leq 0.05$  using a paired ttest comparing numbers of dsRed<sup>+</sup> cells on days post irradiation to the first detected number of on day 15. Data are mean and standard error.  $N=5$  for Sublethal Shielded;  $N=4$  for Sublethal Unshielded;  $N=3$  for Lethal Unshielded.

Microglia derived from donor BM in these experiments were DsRed<sup>+</sup>, as were all hematopoietic cells derived from the donor marrow. In addition, activated microglia may not be easily distinguishable from other hematopoietic cell types by their morphology alone. To distinguish transmigrated cells from cells that temporarily adhered to the vascular wall in these experiments time-lapse images were acquired. **Figure 5** consists of two images taken 3 minutes apart on day 28 post irradiation. These images clearly show BMDCs that temporarily adhere (asterisks) as well as cells that have transmigrated (arrowheads).

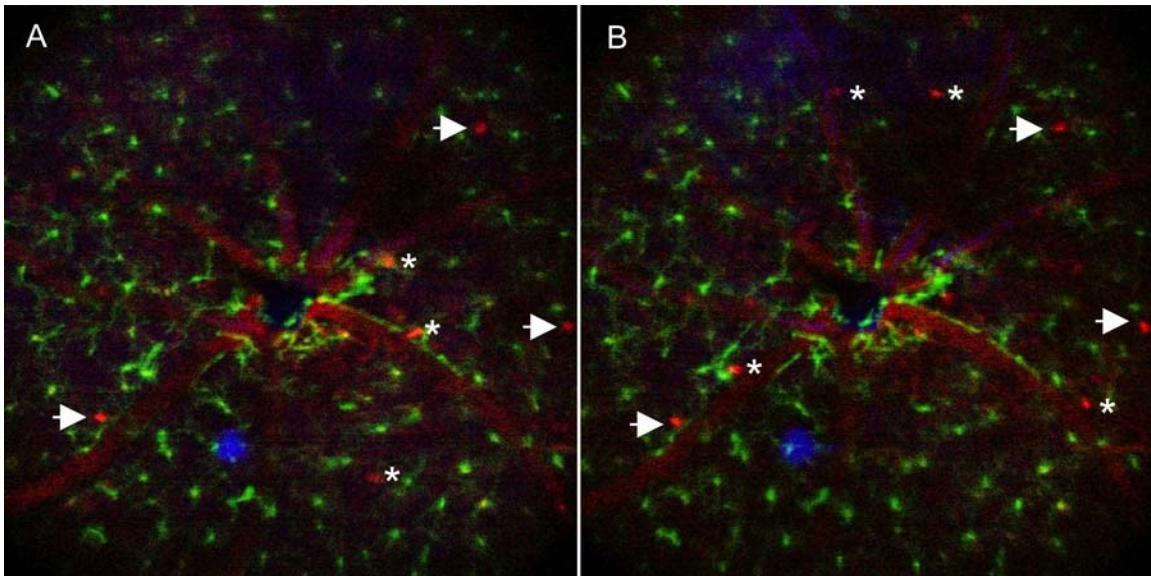


**Figure 5.** Time-lapse images taken at  $t = 0$  min (**A**) and  $t = 3$  min (**B**) apart on day 28 post irradiation. Donor DsRed cells that are engrafted are indicated by arrowheads; these cells can be identified in both frames. Asterisks identify donor cells that were only temporarily adherent; these cells are only found in either frame.

The mechanism of loss of resident microglia as shown in **Figures 3 and 4** is still to be determined. Z stack analysis of an irradiated retina three months after irradiation showed that resident GFP<sup>+</sup> were found throughout retinal layers (**Figure 6 a, b**), but donor microglia were found in the inner retina in proximity to the vasculature (**Figure 6a**), suggesting that donor cells are recruited to the damaged retina through the breached BRB of the vascular endothelial wall. The enlarged area of **Figure 6a** highlights the characteristic morphology of a donor DsRed ramified microglia. Further studies on the fate of the resident microglia are being conducted.

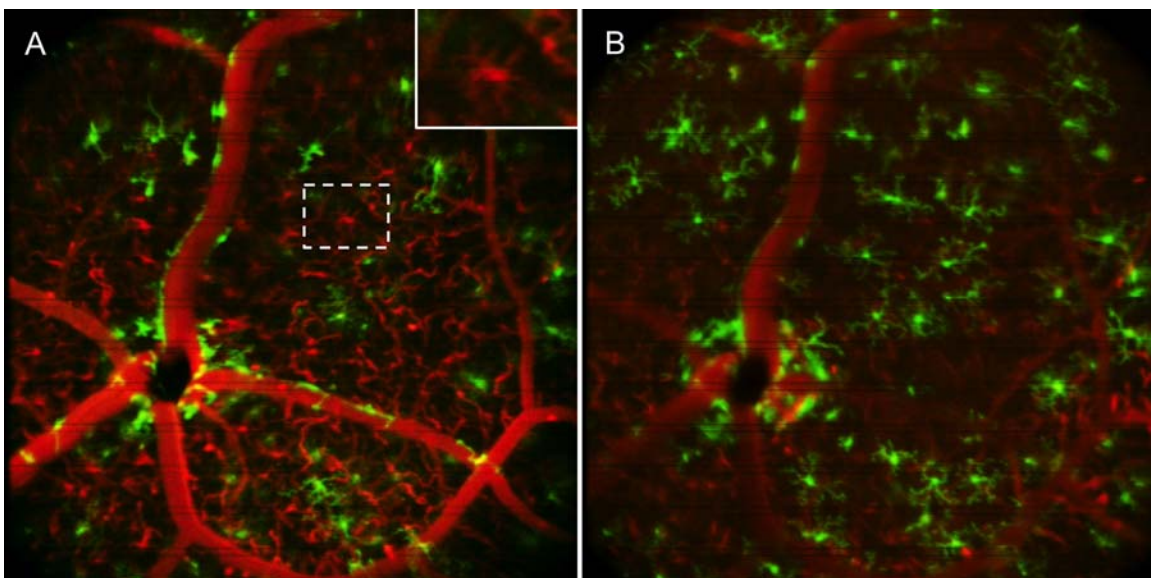


**Figure 6.** Images from an *in vivo* z-stack three months after irradiation and BM transplantation. **A)** inner retina. A population of resident GFP<sup>+</sup> and donor DsRed microglia are found in the same plane as the vascular layer. DsRed<sup>+</sup> cells are difficult to differentiate from other blood cells, because the blood has been reconstituted from the DsRed<sup>+</sup> bone marrow transplant. The

*inlay shows an enlarged DsRed+ cell (box in A) that exhibits typical morphology of a ramified microglia. B) Image about 20 μm posterior to (A). Mainly GFP+ microglia reside at this depth.*

### **Significance**

We have used *in vivo* retinal imaging a) to evaluate the integrity of the blood-retinal barrier and b) to simultaneously track and quantify the numbers of resident retinal microglia and engrafting BMDC as a function of exposure to gamma radiation. Our results indicate that direct radiation affects BRB integrity, survival of resident microglia and engraftment rate of BMDCs.

Dose-dependent loss of resident microglia was observed when mice were irradiated without a protective headshield. With sublethal irradiation, transient loss of resident microglia was observed. With lethal irradiation, progressive loss continued to the end of the experimental period. In either case, it took weeks for the loss to be detected. The engraftment of BMDCs lagged further behind the loss of the resident cells by approximately a month in lethally irradiated mice. This period of relative microglia depletion may contribute to the development of posterior chamber complications that have been reported in BM transplant patients [3,4]. Our FLA experiments demonstrated that even sublethal irradiation conditions induced a compromised BRB. Other reports have suggested that compromised BRB is necessary for efficient BMDC engraftment [5,6]. Consistent with the role of a breached BRB in BMDC engraftment, we found DsRed donor cells mainly in proximity to small vessels in the inner retina. Consistent with other studies, our data demonstrate that replacement of endogenous microglial population with BMDCs requires direct irradiation of the eyes. Taken together with previous studies, [5,6] we also conclude that studies that utilize ionizing radiation to prime engraftment of bone marrow derived cells do not measure homeostatic microglial turnover, but instead measure response to radiation-induced injury.

Future studies will be needed to clarify whether the observed vascular and cellular changes are associated with damage to photoreceptors or retinal ganglion cells (and by implication, CNS neurons), and whether the damage is further exacerbated by the inflammatory cascade. If that is the case, it may be important to consider neuroprotective strategies for individuals subjected to radiation exposure.

### **Publications and Abstracts**

Alt C, Runnels JR, and Lin CP. *In Vivo* Imaging of Blood Retinal Barrier Integrity and Microglia Response after Ionizing Radiation. Submitted.

### **Patents from this award**

None

### **References**

- 1) H. Xu, M. Chen, E.J. Mayer, et al., Turnover of Resident Retinal Microglia in the Normal Adult Mouse, *GLIA* **55**:1189–1198 (2007).
- 2) H. Kaneko, K.M. Nishiguchi, M. Nakamura, et al., Characteristics of Bone Marrow–Derived Microglia in the Normal and Injured Retina. *IOVS* **49**: 4162-4168 (2008).
- 3) S.J. Moon and W. F. Mieler. Retinal complications of bone marrow and solid organ transplantation. *Curr. Opin. Ophthalmol* **14**:433–442 (2003)
- 4) N.M. Coskuncan, D.A. Jabs, J.P. Dunn, et al., The Eye in Bone Marrow Transplantation VI. Retinal Complications. *Arch. Ophthalmol.* **112**: 372-379 (1994).
- 5) P.S. Muether, I. Semkova, K. Schmidt, et al., Conditions of Retinal Glial and Inflammatory Cell Activation Following Irradiation in a GFP-chimeric Mouse Model. *IOVS*, Apr. 30, 2010.
- 6) A. Mildner, H. Schmidt, M. Nitsche, et al., Microglia in the adult brain arise from Ly-6ChiCCR2+ monocytes only under defined host conditions. *Nat. Neuroscience* **10**:1544-1553 (2007).

## 9. Principal Investigators: G.J.Tearney, MD, Ph.D, B.E. Bouma, Ph.D.

**Project Title:** Wide-field superresolution microscopy

### Objective

Recently, a revolution in optical microscopy has taken place, opening up the possibility of sub-diffraction limited fluorescence imaging, also termed nanoscopy [1]. These advances have taken the names of photo-activated localization microscopy (PALM), stochastic optical reconstruction microscopy (STORM) [2, 3] and stimulated emission depletion (STED) [4, 5]. Both techniques have provided incredible images of sub-cellular detail with resolutions approaching 20 nm, previously only observable by electron microscopy [4, 6]. This excitement has been dampened by limitations of these techniques. PALM/STORM requires special photoswitching fluorophores and acquisition of many images prohibiting the imaging of living organisms. STED works faster [4] with regular fluorophores but relies on the integrity of an intense donut beam to depopulate excited states. These limitations prevent sub-diffraction imaging deep into tissues, as aberrations in tissue destroy the shape of the donut beam.

### Approach

Our idea, termed Speckle Super-resolution Microscopy (SSM), involves the use of laser speckle patterns to deplete excited molecules back to their ground states, through the process of stimulated emission and depletion, after they have been excited by a separate laser in a wide-field configuration. The advantage of using speckle is that unlike a scanning STED microscope, a coherent speckle pattern retains a strong zero-intensity null, even in the presence of a high degree of scattering deep into tissue. In addition, due to these strong nulls, the effective saturation factor can be 2 orders of magnitude higher than that of the donut beam [7].

Unlike PALM/STORM, the process is not stochastic, i.e. most of the fluorophores within the nulls remains in excited state, resulting in a much higher SNR. Moreover, a bleaching stage-activation cycle is not required. With SSM, the nulls can be changed immediately by just altering the speckle pattern. Figure 1 shows a simulation that explains this concept. A fully developed speckle pattern is shown in (A), demonstrating the characteristic graininess seen when illuminating a scattering substance with a coherent laser. Imagine that the speckle pattern illuminates a uniformly fluorescing sample such that fluorescence of most of the sample depleted through stimulated emission, as shown (B). In this case most of the fluorophores within the locations represented by the nulls (black spots) remain in excited state and ready to fluoresce. These dark spots are generally separated from each other by more than the diffraction limit, and thus their locations are individually resolvable with great precision using similar fitting procedures to those employed in PALM/STORM. The locations of the dark spots can be easily changed to create a new pattern by altering the illumination's angle of incidence or creating a new speckle pattern (e.g. C, D). The process can be repeated to compile an image. Wide field imaging and optical sectioning can be accomplished by the

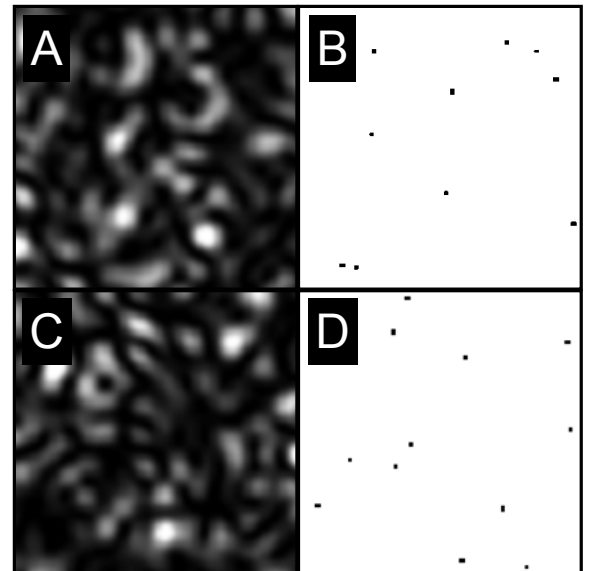
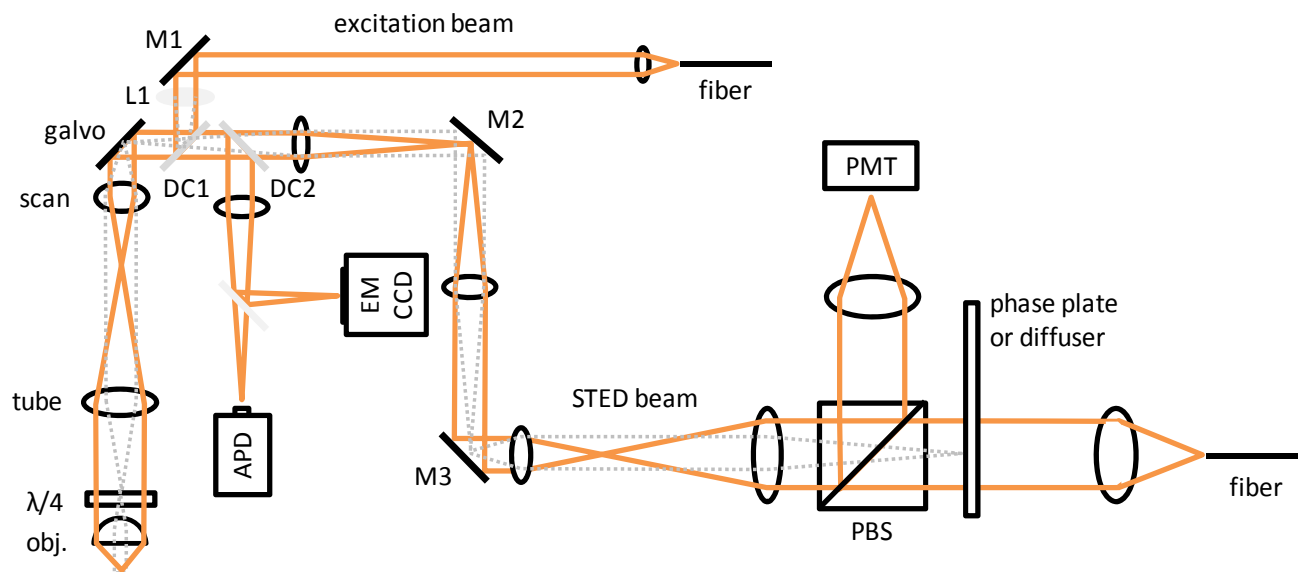


**Figure 1.** Fully developed laser speckle pattern. B. Nulls (-40 dB) for speckle pattern in (A). C. Different speckle pattern. D. Nulls (-40 dB) for speckle pattern in (C).

method of Mertz et al., [8] by measuring the variance of the speckle pattern as it is changed over time. Super-resolution in the axial direction may also be possible by using the astigmatism STORM approach recently demonstrated by Zhuang et al. [6] The peak power requirements for wide field SSM are greater than that of STED. In order to achieve significant STED action, the peak pulse energy density generally needs to be on the order of 10-100 MW/cm<sup>2</sup>. Common pulsed lasers with sufficient peak power will easily suffice when the light is focused to a single spot with a high (NA > 1.0) lens. With SSM, an extended field is illuminated, diminishing the irradiance by at least the square of the illuminated field diameter. The increased power requirements for SSM will therefore require additional laser development. However, we are encouraged by reports of Hell et al. showing that STED action can be attained at far lower average powers by utilizing triplet state relaxation (TRES)[9]. The improved saturation factor found with speckle illumination helps here as well by diminishing the power requirements further. Nevertheless, if wide field SSM is intractable due to the unavailability of appropriate laser sources, SSM can be conducted in a point scanning mode using conventional pulsed lasers and multiple or multianode (i.e. quadrant) detectors.

### Accomplishments

A microscope was built and images were acquired to demonstrate the potential of Speckle Superresolution Microscopy.



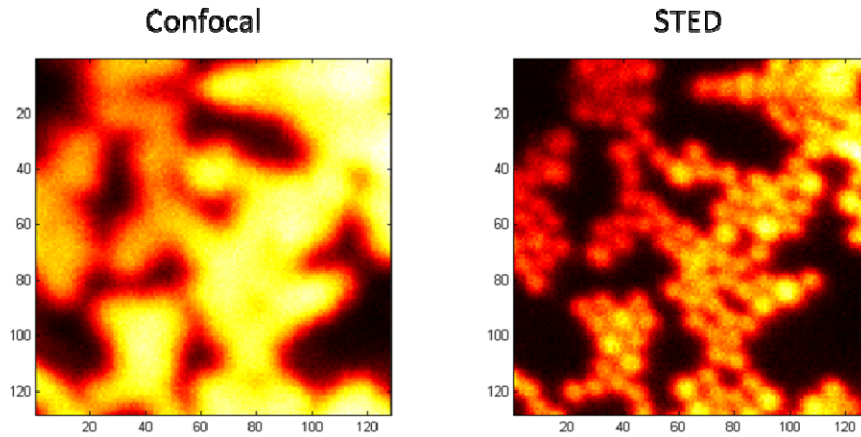
**Figure 2.** Super-resolution microscopy set-up. The set-up can be switched between the standard STED microscope and wide-field SSM modes. For SSM mode L1 lens is inserted and a phase plate is replaced with a diffuser. A flipper mirror is used to direct fluorescence onto EM-CDD. PMT is used to monitor STED and excitation beam spatial alignment. obj. – objective lens;  $\lambda/4$  – quarter waveplate; tube – tube lens; scan – scan lens; galvo – a pair of galvanometric scanning mirrors; DC1, DC2 – dichroics; M1-3 – mirrors; APD – avalanche photodiode; EM-CDD – electron multiplied CCD camera; PMT – photomultiplier tube; PBS – polarizing beamsplitter;

Figure 2 shows a super-resolution microscopy set-up that was assembled and can function both as a standard scanning STED and speckle STED microscope. The dual configuration, which can be easily interchanged, is necessary to compare quantitatively the performance of the two super-resolution techniques. Moreover, the standard scanning STED microscope has a pair of galvanometric mirrors, which might be used in a scanning SSM approach if it proves to be necessary, as discussed above. Scanning is also useful to align and characterize the system, as demonstrated below. Excitation and

depletion (STED) beams are derived from mode-locked Ti:sapphire laser (not shown in Figure 2), similar to that of Ref [10], and brought to the set-up through appropriate single mode fibers. The two beams are overlapped by the help of dichroics, lenses, arranged in 4-*f* system, and mirrors. The beams are scanned with a pair of galvanometer mirrors and fluorescence is descanned and detected with an avalanche photodiode (APD).

To turn the system into the SSM, a phase plate is replaced with a diffuser, which randomizes the phase of collimated STED beam effectively making each ray in the beam divergent, as shown by gray dotted lines in Figure 2. The STED beam illumination becomes wide field, in a form of speckle pattern (see Figure 4 and Figure 5 for reference), at the focus of the objective lens. In order to match the size of excitation beam illumination to that of the STED speckle pattern, a lens, L1 (see Figure 2) is inserted in the excitation beam path. The detection is switched from APD to EM-CCD by means of a flipper mirror.

The system can function as a confocal microscope when in a standard STED mode by simply blocking the STED beam. Figure 3 illustrates the performance of confocal versus STED microscopy. A cluster of 200 nm beads becomes resolvable in the STED images demonstrating a significant resolution improvement.



**Figure 3.** Confocal versus standard STED microscopy. Images shows that STED microscopy improves resolution by resolving 200 nm fluorescing beads.

In order to form a fully developed speckle pattern to be used in SSM, a laser with a long coherence length is necessary. Figure 4 shows a speckle pattern formed by cw and pulsed operation of ti:sapphire laser respectively, as measured with a CCD camera right after the diffuser. The patterns shows high similarity and fully developed speckles [11], which means that pulsed radiation can be used for SSM despite its rather short coherence length ( $\sim 50\mu\text{m}$ ). This is important since pulsed radiation has higher peak power and helps to avoid fast photobleaching compared to cw radiation [9,12].

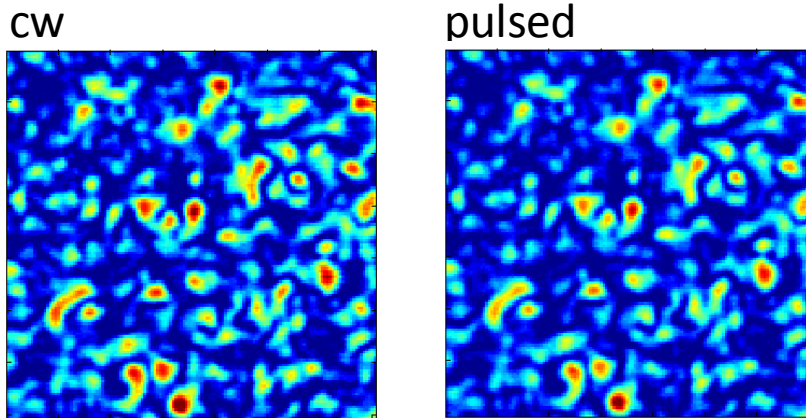


**Figure 4.** Speckle pattern formed with cw and pulsed (mode-locked) operation of ti:sapphire laser as recorded with CCD camera.

A speckle pattern formed in the sample plane had to be kept relatively small ( $\approx 3 \mu\text{m}$ ) in order to maintain high illumination intensity for efficient fluorescence depletion. Figure 5 shows speckle patterns obtained by scanning a single 150 nm gold bead, which represents a true electrical field distribution under a high NA objective focusing conditions [13, 14]. The scattered signal was detected with a PMT shown in Figure 2. The diffuser was moved with each acquisition by a distance necessary to form a new uncorrelated speckle pattern. The images also show that the speckle patterns have largely retained the ability to form zero intensity regions despite depolarization effect that can generate axially oriented polarization component (NA=1.2) [14,15].

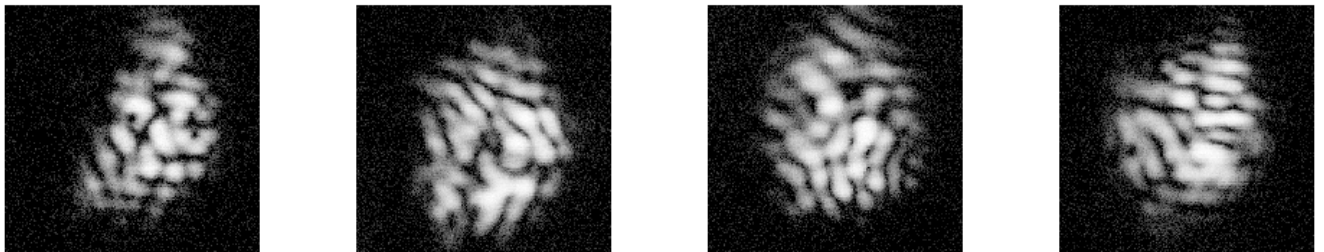


**Figure 5.** A series of speckle pattern images on a logarithmic scale (4db) formed at the objective sample plane. It shows that zeros are formed in parts of the images and the speckle patterns are uncorrelated to each other. Image size:  $6 \times 6 \mu\text{m}$ .

Fluorescence can be switched off (depleted), with the speckle pattern shown above, in various parts of sample. As illustrated in Figure 6, two recorded fluorescence images of the same 200 nm beads sample have been immersed in another dye demonstrate different image structures due to different depletion structures. The difference between the two images is shown in the differential image obtained by subtracting one image from another.

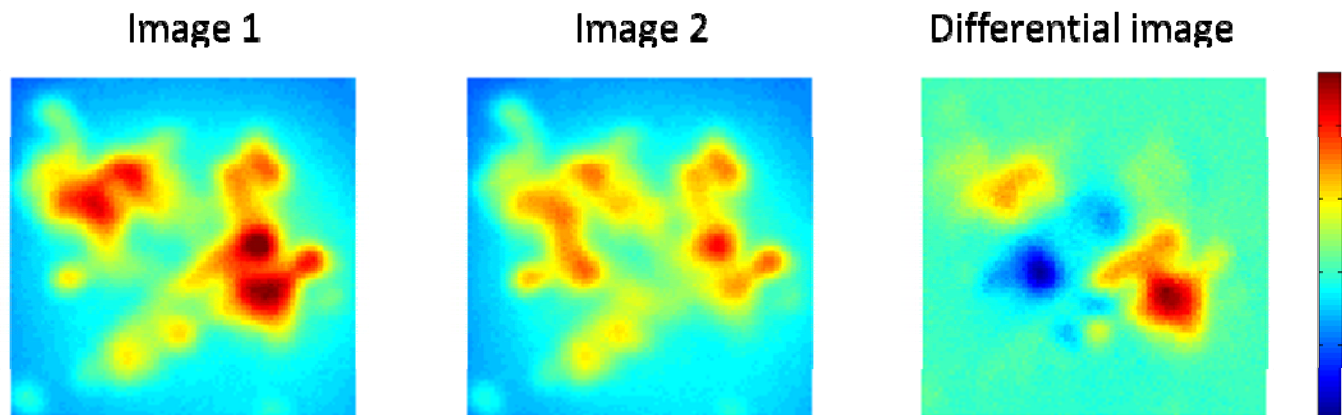


**Figure 6.** Two fluorescence images (1&2) recorded with different speckle STED beam. The differential image shows areas where the depletion takes place.

Fluorescence can be almost completely switched off if the intensity of speckle pattern is high enough. Figure 7 shows fluorescence intensity variation in one selected pixel, in a separate experiment, when a speckle pattern is changed. We can see that the fluorescence reduction (depletion) can be as high as 10 times, which suggests that the resolution can potentially be significantly improved with this STED beam intensity levels [16] over the whole area.

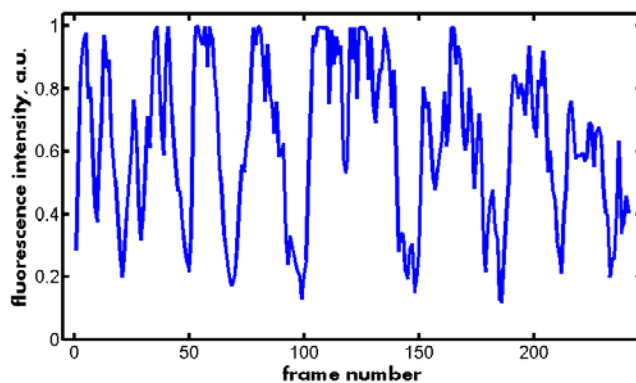


**Figure 7.** Fluorescence intensity depletion in one selected pixel as function of frame number. Fluorescence depletion by a factor of 10 can be achieved.

In case of a sample of dispersed fluorescent nanobeads, the entire bead can be effectively switched off and on again by changing the speckle pattern, as illustrated in Figure 8. Bead blinking is then observed with each acquired frame. Regularly, hundreds of images were acquired in order to be able to reconstruct a final image, with each image exposed to a different and mutually uncorrelated speckle pattern. To minimize photobleaching, due to continuous excitation and high STED intensities used, exposure time had to be minimized and illumination shut off whenever camera was not recording (for instance when a diffuser was moved to different position). The whole process had to be carefully synchronized in order to avoid recording when, for example, the diffuser is moved, and to shorten the total acquisition time. Each image in Figure 8 was acquired with 40 msec exposure, which was long enough to achieve the satisfactory signal to noise ratio due to the sensitive EMCCD camera used. Short integration time was also necessary because of a limited dynamic range of the camera. Relatively high excitation

intensity was found to be necessary in order for STED beam to efficiently deplete fluorescence (rather than excite it). As it is apparent from Figure 8, the photobleaching is not significant due to the fast acquisition. The acquisition time was set to 10 msec in this particular experiment. The images recorded with this setting were shifting slightly from frame to frame due to vibrations in the system.

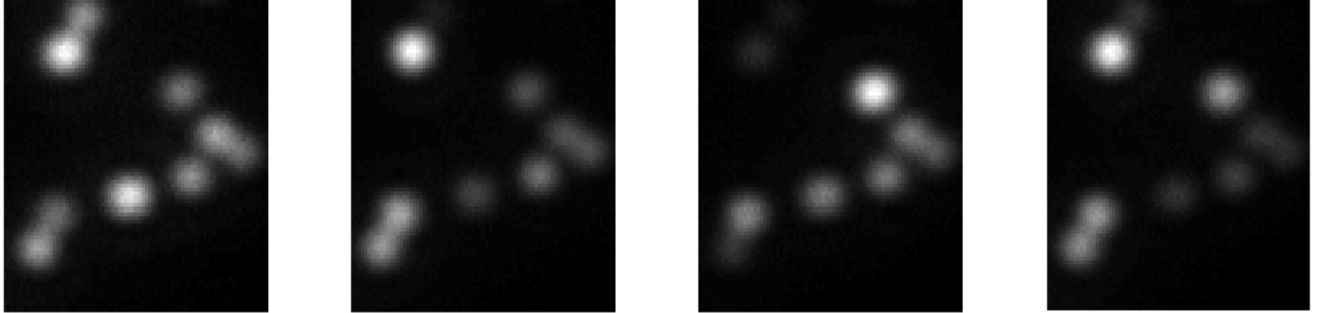


**Figure 8.** A series of consecutive fluorescence images showing that fluorescence can be switched on and off in various places because of depletion. Image size:  $4.2 \times 6 \mu\text{m}$

We are currently working on minimizing vibrations in order to get stable images, which is essential in superresolution imaging. Further to that end, we are developing an image processing algorithm that will reconstruct a superresolved image from the recorded series of images. The algorithm will be based on similar techniques used in STORM [3] and dynamic speckle illumination microscopy [8] techniques, as described above. As a demonstration of a simple reconstruction algorithm, we can directly apply the later technique, which is essentially taking a standard deviation of the stack of images, to generate a final image with rejected background, as illustrated in Figure 9.

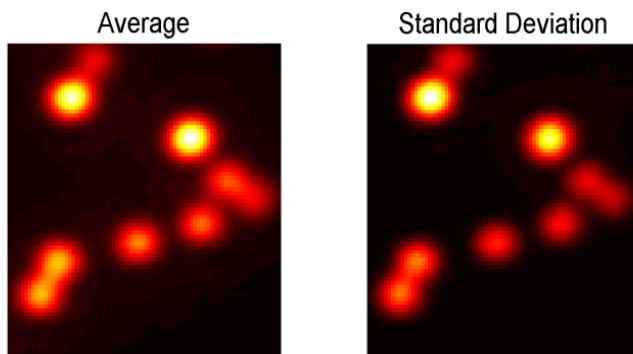


**Figure 9.** Mean and standard deviation images illustrating a background rejection capability similar to ref. [8]. Image size:  $4.2 \times 6 \mu\text{m}$

In addition we are planning to implement an amplified ti:sapphire system to generate a more intense speckle pattern illumination on a sample. Pulse energy of up to 1000 times higher would be available, which would enable efficient depletion over 1000 time bigger area than currently used, that is  $100 \times 100 \mu\text{m}$  compared to the current  $3 \times 3 \mu\text{m}$ . The higher intensities will also be crucial for trying to image deeper in tissue with SSM technique, which is the final goal of this project.

## Significance

A technique capable of providing sub-diffraction limited imaging of intact or living tissues would open up a much greater number of possibilities for nanoscopy in the biological sciences. When applied to problems in military medicine, for example, deep tissue nanoscopy in animal and human studies could provide an improved understanding of the molecular mechanisms of TBI and wound healing.

## Publications and Abstracts

None

## Patents filed for inventions funded, in whole or part, by Military Medicine (AFOSR)

Patent Application no. 12/69356

## References

1. S. W. Hell, "Toward fluorescence nanoscopy," *Nature biotechnology* **21**, 1347-1355 (2003).
2. E. Betzig, G. H. Patterson, R. Sougrat, O. W. Lindwasser, S. Olenych, J. S. Bonifacio, M. W. Davidson, J. Lippincott-Schwartz, and H. F. Hess, "Imaging intracellular fluorescent proteins at nanometer resolution," *Science* **313**, 1642-1645 (2006).
3. M. J. Rust, M. Bates, and X. W. Zhuang, "Sub-diffraction-limit imaging by stochastic optical reconstruction microscopy (STORM)," *Nat. Methods* **3**, 793-795 (2006).
4. V. Westphal, S. O. Rizzoli, M. A. Lauterbach, D. Kamin, R. Jahn, and S. W. Hell, "Video-rate far-field optical nanoscopy dissects synaptic vesicle movement," *Science (New York, N.Y)* **320**, 246-249 (2008).
5. K. I. Willig, S. O. Rizzoli, V. Westphal, R. Jahn, and S. W. Hell, "STED microscopy reveals that synaptotagmin remains clustered after synaptic vesicle exocytosis," *Nature* **440**, 935-939 (2006).
6. B. Huang, W. Wang, M. Bates, and X. Zhuang, "Three-dimensional super-resolution imaging by stochastic optical reconstruction microscopy," *Science (New York, N.Y)* **319**, 810-813 (2008).
7. B. Harke, J. Keller, C. K. Ullal, V. Westphal, A. Schonle, and S. W. Hell, "Resolution scaling in STED microscopy," *Optics express* **16**, 4154-4162 (2008).
8. C. Ventalon and J. Mertz, "Quasi-confocal fluorescence sectioning with dynamic speckle illumination," *Opt Lett* **30**, 3350-3352 (2005).
9. G. Donnert, J. Keller, R. Medda, M. A. Andrei, S. O. Rizzoli, R. Lurmann, R. Jahn, C. Eggeling, and S. W. Hell, "Macromolecular-scale resolution in biological fluorescence microscopy," *Proc. Natl. Acad. Sci. U. S. A.* **103**, 11440-11445 (2006).
10. E. Auksoorius, B. R. Boruah, C. Dunsby, P. M. P. Lanigan, G. Kennedy, M. A. A. Neil, and P. M. W. French, "Stimulated emission depletion microscopy with a supercontinuum source and fluorescence lifetime imaging," *Optics Letters* **33**, 113-115 (2008).
11. J. W. Goodman, "Some fundamental properties of speckle," *Journal of the Optical Society of America* **66**, 1145-1150 (1976).
12. J. J. Sieber, K. I. Willig, C. Kutzner, C. Gerding-Reimers, B. Harke, G. Donnert, B. Rammner, C. Eggeling, S. W. Hell, H. Grubmuller, and T. Lang, "Anatomy and

dynamics of a supramolecular membrane protein cluster," *Science* **317**, 1072-1076 (2007).

13. D. Ganic, X. Gan, and M. Gu, "Focusing of doughnut laser beams by a high numerical-aperture objective in free space," *Opt. Express* **11**, 2747-2752 (2003).
14. K. Bahlmann and S. W. Hell, "Depolarization by high aperture focusing," *Appl. Phys. Lett.* **77**, 612-614 (2000).
15. R. Dorn, S. Quabis, and G. Leuchs, "Sharper Focus for a Radially Polarized Light Beam," *Phys. Rev. Lett.* **91**, 2339011-2339014 (2003).
16. B. Harke, J. Keller, C. K. Ullal, V. Westphal, A. Schoenle, and S. W. Hell, "Resolution scaling in STED microscopy," *Opt. Express* **16**, 4154-4162 (2008).

**10. Principal Investigators:** B.E. Bouma, Ph.D., G.J. Tearney, M.D. Ph.D.

**Project Title:** Guided Needle Placement for Vascular Access

### **Objective**

Obtaining vascular access is of critical importance in many medical scenarios. In a trauma setting, obtaining vascular access can mean the difference between life and death for a patient in need of life-saving fluids and medications. This is especially true in field-based medicine where obtaining vascular access is often complicated by environment, stress, and lack of extra medical supplies. In addition, vascular access obtained incorrectly can lead to complications such as inflammation, thrombosis, and infection. Since manual palpation may often be the only cue for determining the optimal position of the needle prior to insertion into a blood vessel, obtaining vascular access is frequently difficult and time consuming. There exists a need for active feedback in needle guidance for obtaining vascular access, particularly in the setting of military trauma.

One promising method for guiding needle placement would be to integrate a sensor within the needle that could identify the proximity of a vessel during insertion and that could specify when the tip of the needle was successfully inserted into a vessel. Our overall goal is to develop an optical sensor that can be incorporated within a needle and that can measure infrared reflectance, birefringence and flow as a function of distance from the tip. The sensor will comprise a passive optical fiber, resident within the needle bore, and a transceiver, roughly the size of a deck of cards, that would provide feedback cues to the operator. The immediate goal of this proposal is to test the principles of our approach and to provide preliminary data for subsequent engineering and development efforts.

### **Approach**

With prior funding, we have developed instrumentation and methods for guiding needle placement in fine needle aspiration (FNA) breast biopsy. [Iftimia et al. 2005] In the breast, differentiation between adipose and fibrous/cancer tissue is an important clinical challenge for reducing the number of non-diagnostic samples in FNA procedures. Our approach to this challenge has been to use a modified FNA needle that contains an optical fiber for sensing tissue reflectance and birefringence using low-coherence interferometry. A recent study developed and tested a differentiation model for adipose and fibrous tissues with an overall classification accuracy of approximately 90%. [Goldberg et al. 2007] Our proposed instrumentation and methods for guiding vascular access will follow from this previous work and will augment the reflectance and birefringence signals with additional measurements of flow through Doppler processing.

Based on our prior experience imaging vessels, we expect that the optical signals from vessel walls and from flowing blood will be easily differentiated from other tissue types.

### Accomplishments

We have further optimized the design and layout of a new miniature laser system (Fig. 2) and obtained images of the ventral surface of a human finger (Fig. 3). The laser operated at 15.3 kHz repetition rate with 12 mW peak output power. The laser could generate 30.4 kHz A-lines rate by utilizing both the forward and backward sweeps.

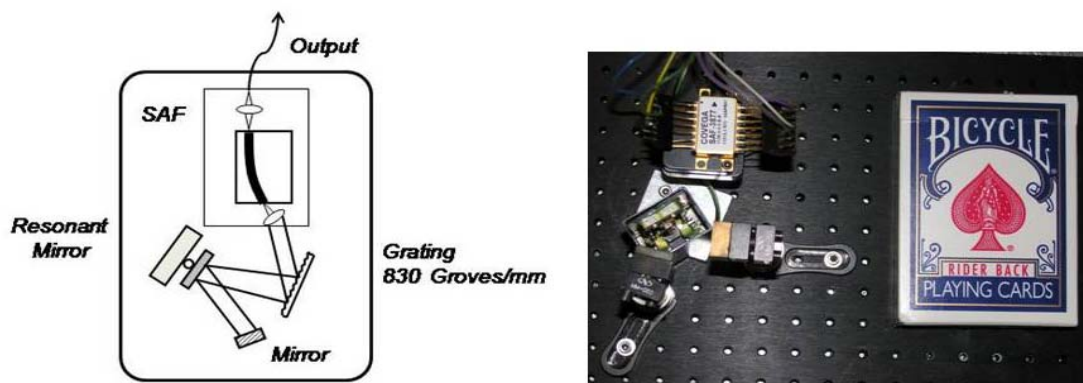
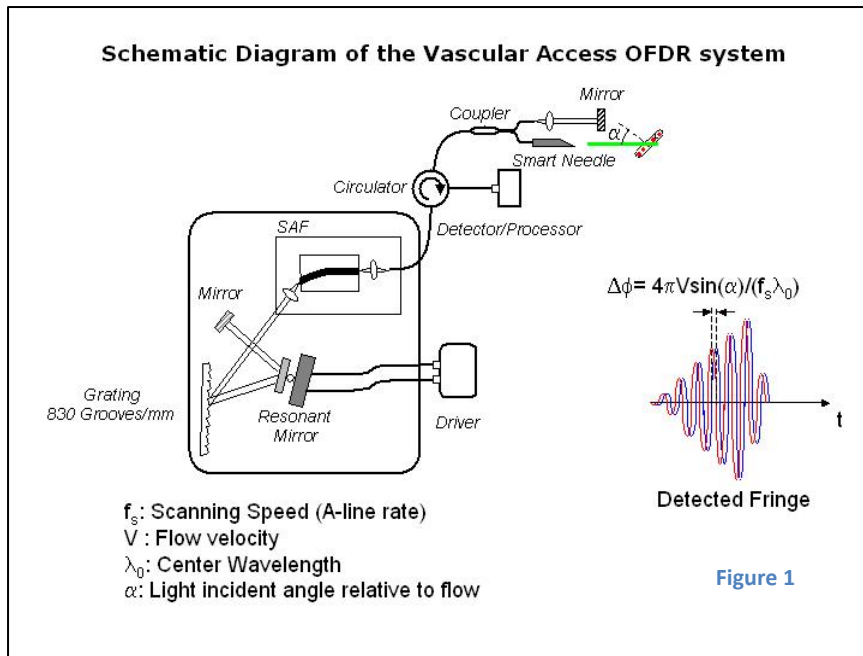


**Figure 2:** Miniature wavelength-swept laser source schematic (left). The output from a semiconductor gain medium illuminates a grating and is deflected via a resonant scanning mirror such that only one wavelength of light is amplified within the laser cavity. As the resonant mirror rotates, the laser's output wavelength is swept in time. A photograph of the source (right) is shown adjacent to a pack of cards for scale.

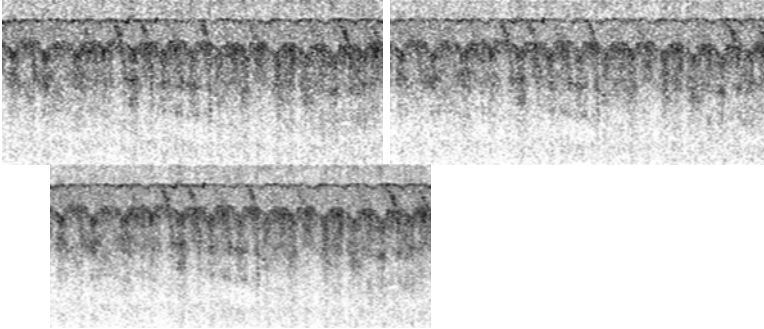


**Figure 3:** 5 mm x 2.25 mm OFDI images from the ventral surface of a human forefinger. Forward (left), backward (middle), and combined (right) wavelength sweep images.

One challenge in building a portable needled guidance device is the large data storage and data transfer demands that are required during high-speed imaging. Therefore, we have investigated the use of reduced bit-depth acquisition for optical frequency domain imaging (OFDI). We found that image acquisition at 8-bit depth allows high system sensitivity with only a minimal drop in the signal-to-noise ratio of  $\sim 0.6$  dB compared with high bit-depth systems (Fig. 4). The use of reduced bit-depth acquisition can be used to increase the system A-line rate with the same data transfer demands, or to reduce the data management requirement for a given system.

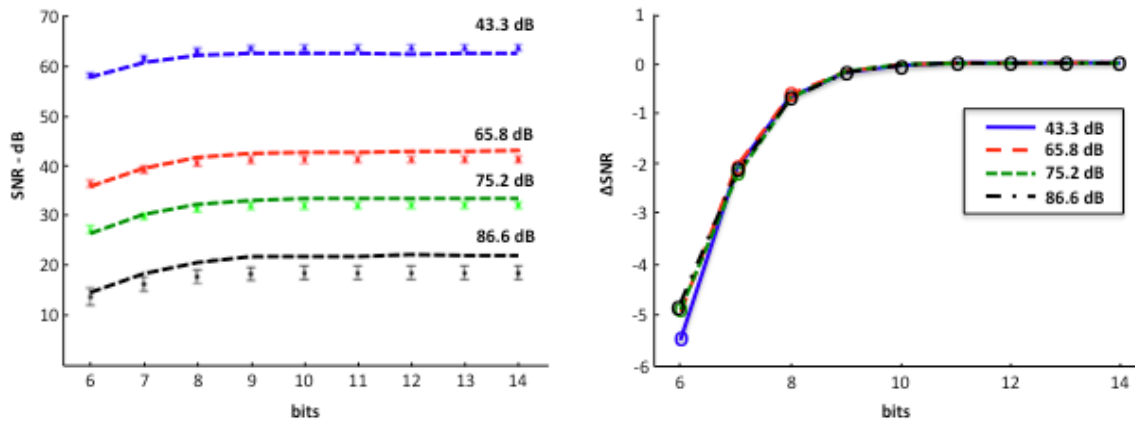


**Figure 4:** SNR as a function of bit-depth from 6 to 14 bits at 1V (left) and change in SNR as a function of bit-depth (right) for four sample arm attenuations (43.3, 65.8, 75.2, 86.6 dB). Acquisition at 8-bit depth provides high system sensitivity with  $\sim 0.6$  dB drop in SNR.

### Significance

In order to achieve a hand-held scale device that could be used for confirmation of vascular access, a miniature, battery-powered swept laser was built and the signal-to-noise ratio was correlated with bit-depth. The laser is capable of video-rate imaging at A-line rates over 30 kHz and with imaging sensitivity near 100 dB, and we have shown that the performance of reduced bit-depth acquisition (8-bit) can achieve high image quality with little drop in SNR compared with higher bit-depth acquisition. These two advances are crucial for reducing data transfer and data management demands and for reducing the form factor of the device. The portable nature of the miniature source and the reduced bit-depth acquisition may also allow OFDR and OFDI technologies to be used in field-based medicine for needle-based vascular confirmation.

## **Patents from this award**

Patent application no. 10/765,430

## **Publications/References**

- Goldberg, B. D., N. V. Iftimia, et al. (2008). "An automated algorithm for differentiation of human breast tissue using low coherence interferometry for fine needle aspiration breast biopsy." *Journal of Biomedical Optics*. **13**(1): 014014.
- Goldberg, BD, SMR Motaghian Nezam, et. al. (2009). "Miniature swept source for point of care Optical Frequency Domain Imaging" *Optics Express*. **17**(5): 3619
- Goldberg, BD, BJ Vakoc, et. al. (2009). "Performance of reduced bit-depth acquisition for optical frequency domain imaging." *Optics Express*. **17**(19): 16968.
- Iftimia, N. V., B. E. Bouma, et al. (2005). "A portable, low coherence interferometry based instrument for fine needle aspiration biopsy guidance." *Review of Scientific Instruments* **76**(6): 064301.

## **11. Principal Investigator: Benjamin Vakoc**

**Title:** Multiparametric optical microscopy of the traumatized brain microenvironment

### **Objective**

The high prevalence of head injuries in the modern battlefield adds specific urgency to a long-standing need for improved therapies for traumatic brain injury (TBI). However, because the underlying mechanisms linking long-term outcome to initial injury are poorly understood, few new and effective therapies have been developed. Thus, many TBI researchers have focused their efforts on understanding these injury-driving mechanisms using mouse and rat models. Intravital imaging techniques capable of revealing key parameters and processes in the TBI microenvironment can dramatically accelerate this discovery process.

We have recently developed an instrument in our lab for assessing the wide-field tumor microenvironment with high temporal resolution. To enable this instrument to study the TBI microenvironment, techniques providing contrast for key physiological parameters and processes in the TBI response are required. The goal of this proposal was therefore to develop and demonstrate in a preliminary manner new techniques for OCT-based mapping of three parameters: blood flow velocity, edema, and brain tissue viability.

### **Approach**

We utilized the following approach to enabling contrast for blood flow velocity, edema, and brain tissue viability.

Blood flow velocity. In previous work, we have enabled OCT-based wide-field and rapid imaging of vascular network morphology through the incorporation of Doppler techniques. However, due to limitations in the Doppler-based technique, the vascular network morphology is revealed absent quantifiable flow velocity information. To enable flow measurements, we focused on the development of new technique that extracts flow velocity from the speckle modulation dynamics.

Edema. Disruption of the blood brain barrier leading to vasogenic edema is a significant complication of TBIs. We explored spectroscopic-based[5] OCT detection of the spectrally varying water absorption coefficient near 1.46  $\mu\text{m}$ .

Viability. We have demonstrated methods for mapping tissue viability in tumor models using intrinsic scattering characteristics. In this aim, we image normal and traumatized mouse brains in vivo to look for correlates of viability to OCT signal.

### **Accomplishments**

We have made significant progress toward quantitative blood flow measurements of the brain during TBI. The ability of OCT to detect the microvascular changes associated with a controlled cortical impact (CCI) TBI model were demonstrated by longitudinal imaging (Figure 1). We have developed and validated a new approach to blood flow measurement based principal component analysis (PCA). The ability of these algorithms to extract flow velocities was tested rigorously in simulations (Figure 2), and in a preliminary manner in vivo in the mouse ear site (Table 1). We are currently refining the blood flow measurement techniques for direct application in vivo. We are also creating a window model preparation of TBI to improve imaging access to the site.

The ability of OCT to detect viability in the brain was evaluated by imaging severe injuries longitudinally. We did not observe similar correlations in scattering to cell death as was present in tumor tissue. Our preliminary conclusion, therefore, is that OCT does not directly provide viability measurements in the brain. Similarly, the application of conventional approaches for spectroscopic water detection have not been successful. Thus, our conclusion has been that OCT is most powerful as a microvascular imaging tool when applied to TBI. We will pursue technical and application development in this area. Through this funding, we established a collaborative relationship with Dr. Michael Whalen (MGH), a pediatrician and active TBI researcher.

### **Significance**

The ability to image modulations in cerebral blood flow due to TBI can have profound implications on the understanding of TBI, and directly guide new therapies. We will focus our efforts on bring this technology to use by developing window models of TBI and studying in these models microvascular perfusion kinetics following TBI in our lab and enabling the labs of Dr. Whalen and Dr. Hamblin (Wellman Center) to use the instrumentation.

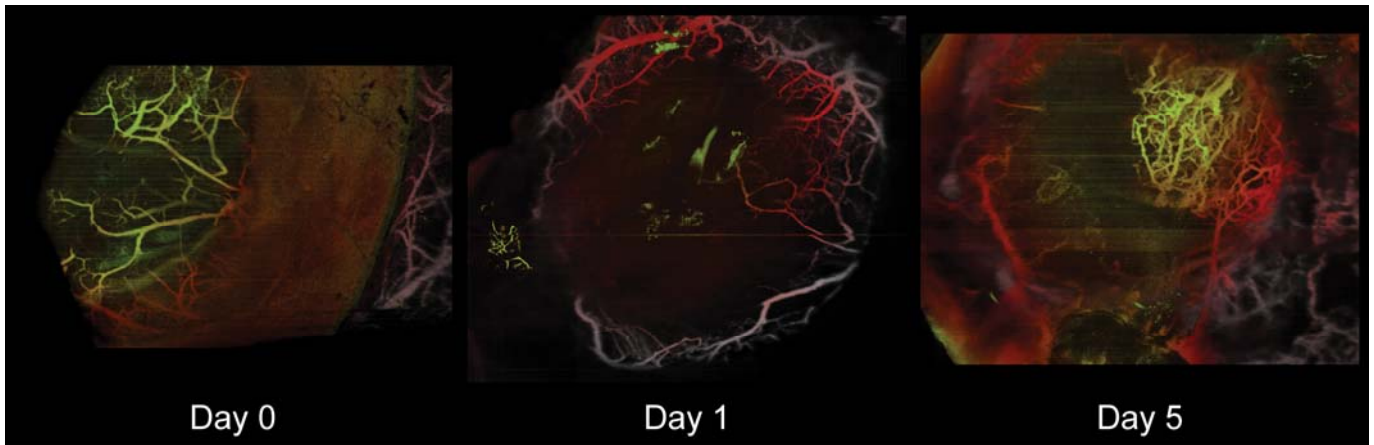


**Figure 1.** We used OCT to monitor the microvascular changes and reduced cerebral blood flow following injury in the same mouse. We also observed neovascularization at Day 5.

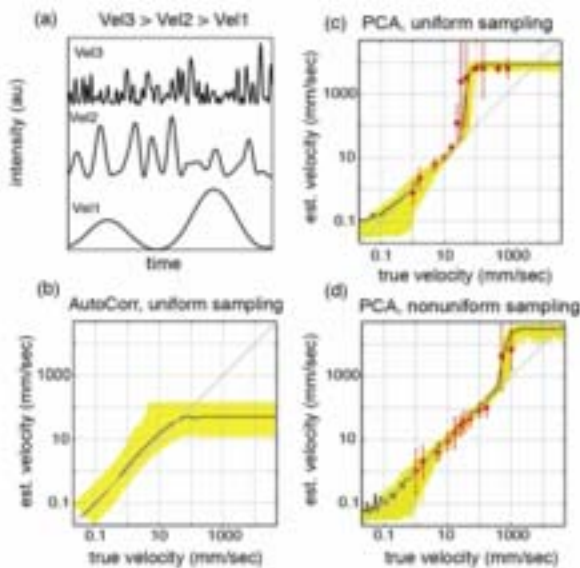


**Figure 2.** Measurement of blood flow velocity using OFDI (a) Simulated OFDI intensity signals are shown for different scatterer velocities. A faster velocity results in a higher frequency signal. (b) Estimation using autocorrelation with a uniform sampling pattern (N=32). The dark line presents the estimate mean, and the yellow band the 10%-90% interval about the mean. (c) Estimation using the PCA method for a uniform sampling pattern (N=32). The dark line presents the mean estimate and yellow band 10%-90% interval. The mean and variance of estimated velocities of a translating rubber phantom using the PCA method are presented in red. (d) Same as in (c) but with the non-uniform sampling pattern (N=32).

Doppler	2.40 <sup>1</sup>	1.37 <sup>2</sup>	12.3 <sup>3</sup>	5.84 <sup>4</sup>	2.00 <sup>5</sup>
PCA	3.30	2.30	8.00	8.28	2.63
Doppler	3.02 <sup>6</sup>	14.2 <sup>7</sup>	3.44 <sup>8</sup>	0.74 <sup>9</sup>	11.1 <sup>10</sup>
PCA	5.58	17.6	8.11	2.61	18.2

**Table 1.** In vivo application of blood flow measurement technique. Estimation of average in vivo flow velocities in the mouse ear using Doppler and newly developed PCA-based methods. Velocities are given in mm/s.

#### Publications/Abstracts

A manuscript detailing the quantitative blood flow measurements using OCT has been submitted to Optics Letters and an oral presentation on the approach was presented at SPIE Medical Imaging conference in February of this year.

#### Patents from this award

None

**12. Principal Investigators:** Andy Yun (P.I.), Charles P. Lin, Georges Tocco\*, Gilles Benichou\*  
Wellman Center for Photomedicine, Dermatology, Massachusetts General Hospital  
\* Surgery/ Transplantation Unit, Massachusetts General Hospital

**Title:** In Vivo Study of Viability and Tolerance for Skin Transplantation

### Objective

The long-term goal of this project is to develop novel skin transplantation methods to help wounded soldiers. While long-term survival/tolerance of vascularized organ transplants, such as kidney and heart, can be relatively easily achieved, presently there is no suitable treatment that would result in the long-term survival of allogeneic skin grafts.

The first specific aim of this project is to test the feasibility of using frozen skin in allogeneic murine models. The second specific aim of this project is to evaluate the effect and mechanism of APC depletion and antibody treatments for long-term graft survival. The third specific aim of this project is to investigate the role of vascularization in skin transplantation and the possibility of promoting tolerance induction in vascularized allografts.

### Approach

We used skin transplantation in mice as a model. We tested two methods to promote prolongation and tolerization of allogeneic skin transplants: (i) use of frozen skin for partial matching; (ii) removal of antigen presenting cells from the donor graft, and (iii) use of skin vascularization at transplantation time combined with tolerization protocols that are known to work in other organ (vascularized) transplants in the same species.

We compared the alloimmunogenicity, susceptibility and cellular trafficking associated with transplantation of fully allogeneic conventional non-primarily vascularized skin grafts and skin allografts vascularized at the time of their placement on mice (vessel anastomoses at time of grafting, see fig. 1).



**Fig. 1:** Vascularized skin flap at the level of the groin area where the donor skin epigastric arteries and veins are anastomosed (end to end for arteries and end to side for veins) to the recipient femoral arteries and veins.

### Accomplishments

#### Use of frozen skin for transplantation in allogeneic murine combinations

We tested 2 different methods for freezing skin, 15% DMSO and 20% glycerol. In our hands, skin frozen in glycerol as a source of skin transplants generated a rejection time and immune response similar to that observed with freshly prepared skins (measured by Elispot analysis, see

fig 2). Ideally, it would be beneficial to have access to an apparatus that enables a gradual freezing of the skin at a rate of 1°C/min to avoid tissue damage due to crystal formation.

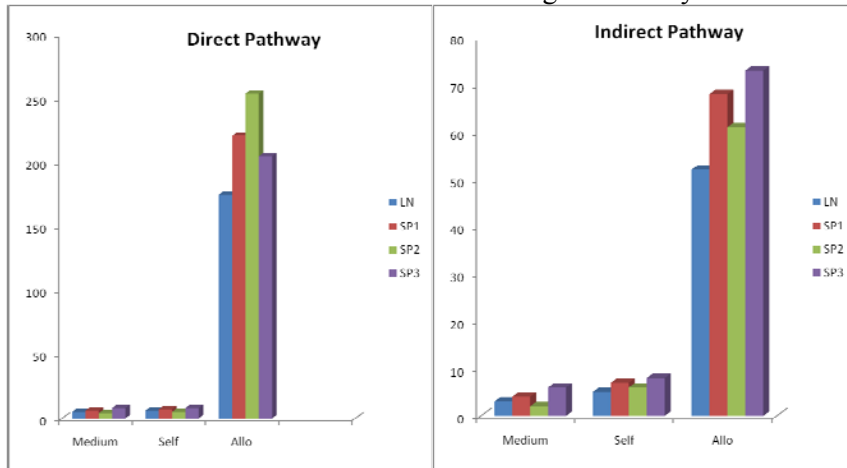


**Fig 2:** IFN $\gamma$  Elispot obtained from cells isolated from spleen and lymph nodes of mice which received a fully allogeneic frozen skin graft 10 days prior.

Evaluate the effects and mechanisms of APC depletion for long-term graft survival

The approach used here was to use CD11c-GFP-DTR transgenic mice as skin donors. These mice carry the receptor for diphtheria toxin on the cells that are positive for CD11c (a specific marker for dendritic cells). Mice do not normally express a receptor for diphtheria toxin, so when Diphtheria toxin is administered to these mice, only the CD11c positive cells are transiently eliminated. However the treatment can only be administered 2 times in a row and the DC population eventually comes back. We used this method to eliminate transiently the CD11c positive cells from the transplant with the idea that this treatment would slow down induction of the immune response (through the direct pathway). Fig 3 shows the elimination of CD11c+ cells after treatment of CD11c-GFP-DTR transgenic mice with diphtheria toxin.

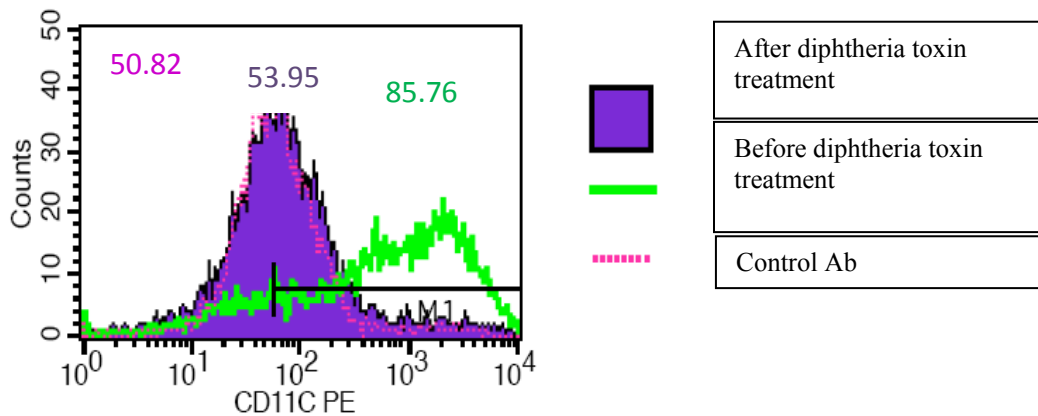


**Fig 3:** Elimination of CD11c<sup>+</sup> cells from spleen 2 days after diphtheria toxin treatment.

While the treatment was successful in eliminating the dermal DCs from the donor skin (observed through in vivo microscopy), it did not delay the rejection nor did it have an impact on the immune response. One possible explanation for this lack of effect might be the fact that the treatment did not eliminate the Langerhans cells from the donor skin (observed through in vivo microscopy). Langerhans cells represent a dendritic cell population present in the epidermis of the skin. We would therefore need to eliminate these cells through another method to ascertain if elimination of donor APCs might prolong/help tolerize skin grafts.

Pre-incubating the skin graft in culture medium before actual transplantation is effective in depleting the graft from DCs. The APCs during the incubation time do migrate out of the graft in the culture medium. This treatment was then successful in delaying the skin graft rejection and preventing activation of the direct pathway (Fig. 4). We would therefore envisage a situation where prior to freezing, skin graft would be pre-incubated in culture medium for 24-48 hours prior.

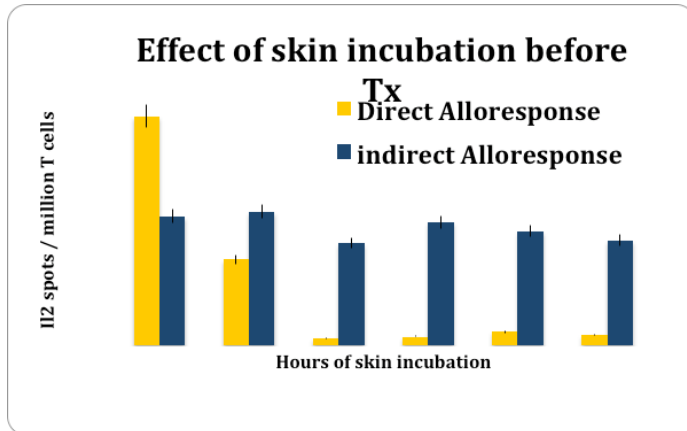


**Fig 4:** Effect of various skin incubation times before transplantation on the generation of a direct response.

Investigate the role of vascularization in skin transplantation and the possibility of promoting tolerance induction in vascularized allografts

We compared the cell trafficking, T cell allorecognition and susceptibility to tolerogenesis in mice transplanted with a fully allogeneic “classical” skin graft and recipients of a skin allograft vascularized at the time of its placement.

First, we evaluated the acute rejection of various skin allografts combinations, vascularized at the time of their placement and conventional, non-primarily vascularized, skin allografts in mice. Vascularized skin grafts were acutely rejected although in a slight but not significantly delayed manner compared to conventional skin grafts (see fig. 5)

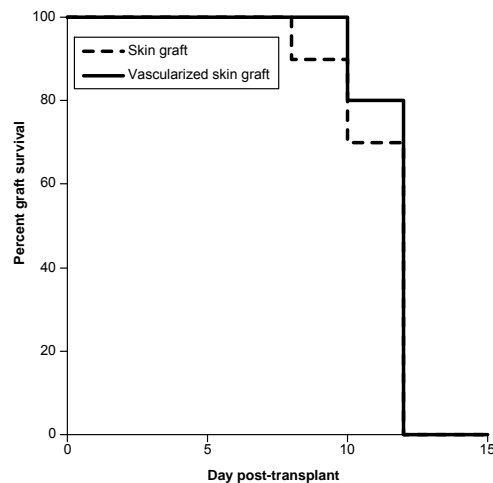


**Fig 5:** Rejection of various fully allogeneic vascularized skin grafts combinations

We observed that graft vascularization at transplantation time is associated with a totally different pattern and kinetics of passenger leukocyte migration (immune cells from the graft. In table 1 are reported the number of passenger leukocytes from the donor that are retrieved in various tissues of the recipient a various time points after transplantation. We observed that after vascularized skin grafts, as early as 1 day post-transplant, passenger leukocytes from the donor are retrieved in all the secondary lymphoid organs that we observed. Contrary to expectations, after conventional skin transplantation, only few passenger leukocytes are retrieved only in the draining lymph node of the recipient and only after 5 days post-transplant.

Days post Tx	Skin					Vasc Skin	
	1	3	5	7	9	1	3
<b>Spleen</b>	0	0	0	0	0	26	54
<b>Thymus</b>	0	0	0	0		0	0
<b>Lung</b>	0	0	0	0		0	0
<b>Liver</b>	0	0	0	0		0	0
<b>Mes LN</b>	0	0	0	0	0	256	80
<b>Draining Ing LN (ipsi)</b>	0	0	8	4	0	6	4
<b>Paraaortic (ipsi)</b>	0	0	0	0	0	0	6
<b>Draining Axill (ipsi)</b>	0	0	6	0	0	42	18
<b>Bracchial (ipsi)</b>	0	0	0	0	0	ND	18
<b>Cervical (ipsi)</b>	0	0	0	0		22	20
<b>Ing LN (contra)</b>	0	0	0	0	0	34	20
<b>Paraaortic (contra)</b>	0	0	0	0	0	6	8
<b>Axill (contra)</b>	0	0	0	0	0	94	38
<b>Bracchial (contra)</b>	0	0	0	0	0	28	14
<b>Cervical (contra)</b>	0	0	0	0		22	20

Vascularized skin transplants are also associated with a different alloresponse by T cells, the recipient immune cells in part responsible for the ultimate rejection of the graft. No indirect response could be measured after vascularized skin transplantation (see fig. 6).

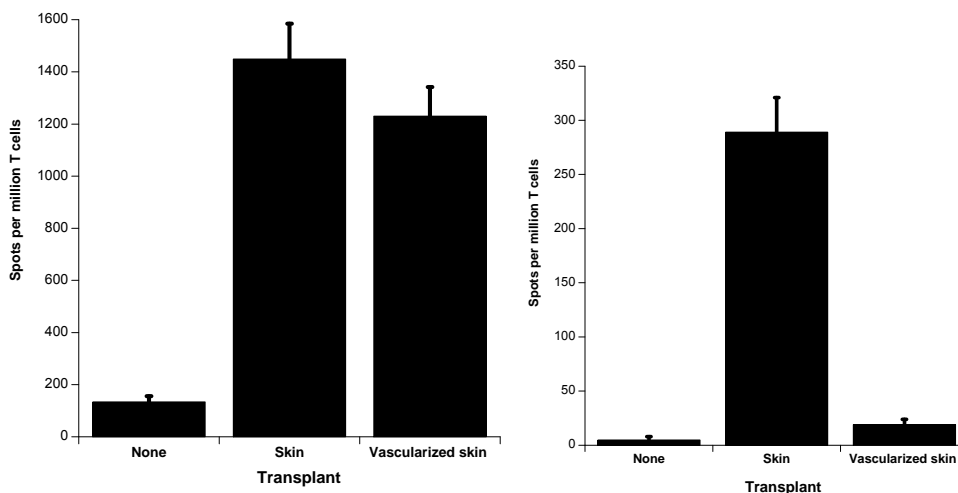


**Fig 6:** Frequency of IL-2 producing T cells activated through the direct and indirect pathways after conventional or primarily vascularized skin transplantation.

In addition, we found that unlike their non-vascularized counterparts, primarily-vascularized skin allografts become infiltrated very early on by large numbers of regulatory T cells (cells specialized in dampening/eliminating the immune response, data not shown).

Finally, we studied the effect of a tolerization protocol known to be effective with heart transplant. Short-term treatment of recipients with anti-CD40L monoclonal antibodies (MR1) has been shown to prolong the survival of heart but not skin allografts. The effect is known to rely essentially on the inhibition of alloreactive CD4+ T cells. First, we compared the effect of anti-CD40L mAbs (0.5 mg injected I.P. at day 0, 2 and 4) on the rejection of non-vascularized skin allografts, vascularized skin allografts and cardiac allografts in the B6 to C3H combination. As expected, anti-CD40L-treatment had no significant effect on the survival of non-vascularized skin allografts. In contrast, preliminary results show that this treatment can markedly extend the survival of vascularized skin transplants.

Vascularized skin allografts can enjoy long-term survival when combined with a short term treatment with an anti-costimulation blockade antibody.

These results bring new insights into the mechanisms by which vascularization influences the immunogenicity and tolerogenicity of allogeneic skin transplants. They open new hopes for one day being able to achieve long-term survival of allogeneic skin grafts for soldiers.

### **Significance**

The results obtained up to now are encouraging about the potential for vascularized skin in achieving long-term graft survival and tolerization. The exact mechanism of the prolonged survival of vascularized graft is unknown at the moment. If successfully developed, vascularized skin transplantation might prove useful to treat wounded soldiers in the battlefield and during rehabilitation.

### **Publications and Abstracts (9/09-12/10)**

- Tocco G., Kim P., Kant CD., Lin C., Yun S., Benichou G., “Cellular Migration in Transplantation Studied Using in vivo Microscopy.”, *Clin Immunol.* 131: S11-12, 2009.
- Tocco G., Kim P., Kant CD., Wynn H, Lin C., Yun S., Benichou G., “The ins and outs of Cellular Migration in Transplantation Revisited through *In Vivo* Microscopy.” *A. J. Trans.* 9: P476, 2009.
- Tocco G., Kant CD., Kim P., Connolly SE., Shea S., Lin C., Yun SH., Benichou G., “Skin Graft Rejection: Direct or Semi-Direct Allorecognition?”, Annual Scientific Exchange December 3-6, 2009, Orlando, Florida.
- Tocco G., Kim P., Kant CD., Lin C., Yun SH., Benichou G., “Allorecognition after Skin Transplantation: Potential for Semi-Direct Pathway?” *A. J. Trans.* 10: P94, 2010.

### **Patents from this award**

None